

Fall 2021

The Development of a Holistic Quality Score Using In-Situ Monitoring of Laser Powder Bed Fusion

Ryan Daigneault

Follow this and additional works at: <https://digitalcommons.georgiasouthern.edu/etd>



Part of the [Industrial Engineering Commons](#), [Manufacturing Commons](#), [Operational Research Commons](#), and the [Other Materials Science and Engineering Commons](#)

Recommended Citation

Daigneault, Ryan, "The Development of a Holistic Quality Score Using In-Situ Monitoring of Laser Powder Bed Fusion" (2021). *Electronic Theses and Dissertations*. 2333.
<https://digitalcommons.georgiasouthern.edu/etd/2333>

This thesis (open access) is brought to you for free and open access by the Jack N. Averitt College of Graduate Studies at Digital Commons@Georgia Southern. It has been accepted for inclusion in Electronic Theses and Dissertations by an authorized administrator of Digital Commons@Georgia Southern. For more information, please contact digitalcommons@georgiasouthern.edu.

THE DEVELOPMENT OF A HOLISTIC QUALITY SCORE
USING IN-SITU MONITORING OF LASER POWDER BED FUSION

by

RYAN JAMES DAIGNEAULT

(Under the Direction of Dean Snelling)

ABSTRACT

Additive manufacturing processes allow for a great degree of flexibility in terms of part production. The process is autonomous once the part has started printing in that the operator generally does not need to intervene until the part is finished. One issue that this introduces, however, is an inability to determine part quality during the printing process. Once a part has started printing, the operator must either wait until the part is finished or regularly check on the part during the print to determine the part quality. Using data gathered from multiple sensors, a quality score can be used to estimate the part quality at any point during the printing process. The development of the score also observed several of the largest contributing ambient factors to both the surface roughness and the part porosity. The largest contributors to quality were the chamber temperature and the oxygen content for the surface roughness and porosity, respectively. Each build characteristic was plotted, and the best fit equations created the quality score. The score generated a zero to one hundred scale that can be easily viewed without intimate knowledge of the process.

INDEX WORDS: Laser powder bed fusion, In-situ monitoring, Oxygen content, Print layer temperature, Chamber temperature, Chamber humidity, Predictive quality score, Data fusion, Sensor integration, Metal additive manufacturing

THE DEVELOPMENT OF A HOLISTIC QUALITY SCORE
USING IN-SITU MONITORING OF LASER POWDER BED FUSION

by

RYAN JAMES DAIGNEAULT

B.S., Georgia Southern University, 2018

M.S., Georgia Southern University, 2021

A Thesis Submitted to the Graduate Faculty of Georgia Southern University

in Partial Fulfillment of the Requirements for the Degree

MASTER OF SCIENCE

THE DEVELOPMENT OF A HOLISTIC QUALITY SCORE
USING IN-SITU MONITORING OF LASER POWDER BED FUSION

by

RYAN JAMES DAIGNEAULT

Major Professor:
Committee:

Dean Snelling
Kamran Kardel
Haijun Gong

Electronic Version Approved:
December 2021

DEDICATION

To my mother Teri, my grandfather Bob, and my dogs Beauregard and Sully

ACKNOWLEDGMENTS

I was given a great deal of support throughout the writing of this work and would like to thank those who helped me.

I would first like to thank my supervisor, Professor Dean Snelling, whose advise and expertise both lead me down the path of my master's and was invaluable to its completion. You provided not only direction but a pacifying voice when problems arose. Your guidance and insight developed me as researcher, and I hope to keep your teachings with me as move forward.

I would like to thank the professors who helped me the most during my time. Dr. Haijun Gong's teachings in the additive field are fundamental to my interest in it. You sparked my interest in 3D printing and I hope to inspire others to work and research the field. Dr. Kamran Kardel provided insightful discussion on process improvement as well as many solutions when having trouble with my understanding of how to do research and write a thesis.

Finally, I would like to thank my family for their motivational attitude and calming demeanor. Without your encouragement I would not be where I am today. I would also like to thank my friends, Beau Ragland and Michael Phillips, you provided well needed breaks and conversation outside my research.

TABLE OF CONTENTS

	Page
ACKNOWLEDGMENTS	3
LIST OF TABLES	6
LIST OF FIGURES	7
CHAPTERS	
1: INTRODUCTION.....	8
1.1 Primary Research Goal	8
1.2 Research Question 1: In-situ Monitoring of Build Aspects	10
1.3 Research Question 2: Equal Comparison of Aspects.....	11
1.4 Research Question 3: The Introduction of a Quality Score	12
1.5 Thesis Format	16
2: LITERATURE REVIEW	17
2.1 Background Research	17
2.2 Image Processing	18
2.3 Multi-Sensor Data Fusion Research	20
2.4 Machine Learning	21
2.2 Presented Thesis Work	22
3: EXPERIMENTAL METHODS	24
3.1 Experimental Preparation.....	24
3.2 Experimental Procedure.....	30
3.3 Part Analysis	31
3.4 Challenges Encountered.....	34
4: RESULTS & DISCUSSION	36
4.1 Print Layer Temperature	36
4.2 Chamber Temperature	38
4.3 Chamber Humidity.....	42
4.4 Oxygen Content	45
4.5 Quality Score	48
CHAPTER 5: CONCLUSION	51
REFERENCES	53
APPENDICES	
A: PRINT LAYER TEMPERATURE DATA	57

B: PRINT LAYER TEMPERATURE STATISTICS	58
C: PRINT LAYER TEMPERATURE BOX PLOTS	59
D: CHAMBER TEMPERATURE DATA	60
E: CHAMBER TEMPERATURE STATISTICS	61
F: CHAMBER TEMPERATURE BOX PLOTS	62
G: CHAMBER HUMIDITY DATA	63
H: CHAMBER HUMIDITY STATISTICS	64
I: CHAMBER HUMIDITY BOX PLOTS	65
J: OXYGEN CONTENT DATA.....	66
K: OXYGEN CONTENT STATISTICS	67
L: OXYGEN CONTENT BOX PLOTS	68

LIST OF TABLES

	Page
Table 1.1: Research Question 1	14
Table 1.2: Research Question 2	15
Table 1.3: Research Question 3	16
Table 3.1: Build Characteristic Ranges.....	31
Table 4.1: Print Layer Temperature Averages.....	38
Table 4.2: Chamber Temperature Averages	42
Table 4.3: Chamber Humidity Averages	45
Table 4.4: Oxygen Content Averages	48

LIST OF FIGURES

	Page
Figure 2.1: Ded Melt Pool Dynamics	21
Figure 3.1: Relationship Schematic	25
Figure 3.2: Sensor Package.....	26
Figure 3.3: Experiment Part Design.....	27
Figure 3.4: Adjustment Package	29
Figure 3.5: Build Setup	30
Figure 3.6: Porosity Collection Diagram	33
Figure 4.1: Print Layer Temperature Average Area Surface Roughness (Sa)	36
Figure 4.2: Print Layer Temperature Average Porosity (%).....	37
Figure 4.3: Chamber Temperature Average Area Surface Roughness (Sa)	39
Figure 4.4: Chamber Temperature Sample 30 Top.....	40
Figure 4.5: Chamber Temperature Average Porosity (%)	41
Figure 4.6: Chamber Humidity Average Area Surface Roughness (Sa).....	43
Figure 4.7: Chamber Humidity Average Porosity (%)	44
Figure 4.8: Oxygen Content Average Area Surface Roughness (Sa)	46
Figure 4.9: Oxygen Content Average Porosity (%).....	47

CHAPTER 1

INTRODUCTION

Part quality has been important in every facet of manufacturing since the very inception of the field. For many decades experts have tried to find a finite definition of the concept of quality however this proved difficult in that each expert would find a definition somewhat like other but one that was more tailored to their ideals. Philip Crosby, who was influential in management and quality theory, defined quality as the “conformance to requirements set by not only the producer but also the customer” (Johnson 2001). On the other hand, foundational thinker Joseph Juran defined quality as being achieved when “a finished product is suitable for use by its intended audience” (Juran 1998). The parallel that can be drawn from most, if not all, definitions of quality are that the customer plays a large role in the determination of the quality requirements. The quality of production in a manufacturing facility determines the number of parts that go through the entirety of the process chain along with the number of parts that get scrapped. In additive manufacturing, quality is an important part of ensuring that each build done generates a usable part. Quality also effects the amount of post processing for parts made with additive manufacturing. Parts made with Laser based Powder Bed Fusion (L-PBF) can see large internal stresses or voids depending on the laser and build characteristics. These defects reduce the effectiveness of the part by introducing issues such as cracking or weakness due to not being fully dense. Reducing these defects is what must be done to work towards improving the quality of the build.

1.1 Primary Research Goal

The goal of this research is to define a part metric-based quality score for Laser-Powder Bed Fusion (L-PBF). At the time of this work, a gap in quality information exists for parts that undergo the printing process. More specifically, once a print is started, the part quality is mostly unattainable until the part has successfully finished and can be examined through non-destructive testing or by sectioning and evaluation. Utilizing various sensors to determine a quality score that allows the user to indirectly analyze quality and even predict final part quality. This can then be used to enhance decisions related to production parts; for

example, terminating a print because the quality is not within the projected range or adjusting print parameters to drive the score to a desired value. The scope of this work was entirely centered on the L-PBF of 316L stainless steel powder. The quality score was generated using numerical data gathered from a custom sensor package including ambient temperature and humidity in the build chamber.

Quality is the sum of many different parts for a process, and this is no different in metal additive. The quality for a metal additive part is determined through many different quality metrics. Some of these metrics are unimportant to some industries and vitally important to others. The scope of the score developed in this work was confined to the part porosity and the surface roughness. These two separate quality metrics are some of the most identifiable for the purposes of part quality. They also provided this work a view of the part quality both internally and externally for porosity and roughness, respectively. These metrics also could be easily tested using the measurement equipment at hand and thus were Excellent candidates for part analysis. With this work looking specifically at two metrics the score was made expandable to include both more sensors and more quality metrics in the future. This would increase the usability of the score by making it more applicable to part quality in different production facilities or by increasing the number of metrics that the quality is shaped by.

Previous work for in process part monitoring in metal additive is almost entirely using per layer imaging or thermal imaging. These methods do well when looking for specific flaws such as voids or incorrect thermal gradients during the print. However, they have not been used to attempt to predict final part quality during the print. Other work has been done using multiple sensors in the metal additive field in Directed Energy Deposition and Powder Bed Fusion as a whole (He et al. 2019). This work used both imaging and non-imaging sources in conjunction to draw a relationship to part quality from thermal gradients from thermal imaging and print bed temperatures. Many of these works cited machine learning as an area of interest moving forward but the majority of the work did not entertain the idea of a predictive monitoring system. While predicted quality has not been worked on in metal additive, CNC machining has been using multiple sensors to predict things such as cutter wear and life. The systems that show the wear

on the cutters in a CNC process use many different sensors taking data during the process to determine this wear value. Stemming from the aforementioned limitations in monitoring and predictive part quality, further investigation was defined through the primary research goal.

Primary Research Goal
To collect fundamental data from a conglomeration of sensors surrounding L-PBF in order to develop an in-situ quality score to gain insight on part quality at any point during a build.

Stemming from the primary goal of the work, several research questions and objectives were created to divide the development of this score into sections.

1.2 Research Question 1: In-situ Monitoring of Build Aspects

Just as all other production processes, L-PBF has many aspects that effect the final part quality. Aspects including oxygen content or print layer temperature can have a large impact on the part such as increased surface roughness or internal stresses. Prior research and tests on individual effects of these build characteristics have been performed and thus information is available on how they affect quality (Sekhar). The simultaneous monitoring of several characteristics at once has been done comparatively much less in this field. By monitoring several aspects an understanding of the relationships to part quality can be drawn and a predictive score can be made. The comparatively limited knowledge on simultaneous multi-aspect monitoring guided the creation of Research Question 1 (RQ1).

Research Question 1
How can multiple build aspects that affect part quality be simultaneously monitored during a print?

There are several methods of taking data on multiple aspects during a print. Hypothesis 1 assumes that an external monitoring system needs to be both developed and integrated onto the additive machine

being used. This counterbalances the short comings of the machine being used in that any aspect that the machine cannot monitor can be added to this external system through an additional sensor. This also allows for a degree of separation between the printing process and the data collection process so that if any glitches were to happen with the additive machine's software, the data can still be collected without interruption.

Hypothesis 1
In order to meet the overall goal of the work, a custom monitoring system must be developed, coded, and implemented to the machine.

1.3 Research Question 2: Equal Comparison of Aspects

The addition of the sensor package to the L-PBF process provided the conduit that led to the development of the quality score through the collection of the aforementioned fundamental data. However, before the quality score can be developed, an experiment must be designed that allows for a direct comparison between all aspects after analyzing the part quality. The aspects of interest are, for the most part, dissimilar to one another. This dissimilarity causes issues in making an equal comparison between all aspects. This issue created the need for Research Question 2 (RQ2) to be asked.

Research Question 2
How can each aspect's effect on each part quality metric be analyzed equally even though the metrics will have different scales, ranges, and units?

To determine the part quality, parts must first be printed and then analyzed. This raises the question of how to design a part where direct comparisons can be made to different part quality metrics for each build aspect. This drives the creation of Hypothesis 2.1. A part must be designed that provides information on the change in both surface roughness and porosity in relation to each build characteristic. The part must

also acknowledge that surface roughness and porosity are two dissimilar metrics and thus must be designed to account for this while allowing for an equal comparison to be conducted.

Hypothesis 2.1
A part must be designed that allows for a look at the change in build aspects versus the change in the part quality in order to compare the effects of the build aspects on the final quality of the part.

Part quality in L-PBF is the total sum of many metrics such as surface roughness, porosity, and internal stresses. These metrics are directly affected by the aspects that can be changed during the print. By adding a sensor package that records in-situ data, the build aspects can be compared to post print part quality metrics. The two metrics desired by this work are the surface roughness and the internal porosity. From prior research it is known that a large contributor to part quality in terms of surface roughness and porosity is the oxygen content in the chamber (Wirth et al. 2021). Hypothesis 2.2 uses this information and assumes that out of the four aspects being tested the oxygen content will provide the largest change to part quality.

Hypothesis 2.2
The oxygen content will show the largest relative change to part quality when compared with the changes from the humidity and the two temperature characteristics.

1.4 Research Question 3: The Introduction of a Quality Score

The concept of predictive quality has previously been used extensively in traditional manufacturing. Mills and lathes have been using this for the determination of tool wear. In the field of metal additive however, this concept is just newly being explored with the emergence of work in in-situ monitoring (Li et al. 2019). The effects of being able to predict the part quality is innately useful to the process. By predicting part quality, processes can be improved in terms of consistency and material usage.

The lack of the involvement of predictive quality determination in this field lead to Research Question 3 (RQ3).

Research Question 3
How can a robust quality score be calculated to provide a predictive view of part quality?

With part analysis comes the influx of information about the part and thus the ability to use that information to compare each aspect change on part quality. By comparing each aspect with respect to one another, the relationships that form between build aspect and part quality can be observed. These relationships form the base of Hypothesis 3. Through the observation of each aspects' relationship to part quality, they can be their own score which, when combined, forms the overall quality score.

Hypothesis 3
The comparison made during the analysis must be used to weight each aspect's in-situ value to calculate individual scores that combine into the overall score.

Table 1.1: Research Question 1

Research Question 1
How can multiple build aspects that affect part quality be simultaneously monitored during a print?
Hypothesis 1
The use of an external monitoring system that can be integrated onto the additive machine will be required.
Methods
<p>A multi-sensor data collection package will be developed to record data of interest from the additive build:</p> <ul style="list-style-type: none"> ● Chamber Temperature ● Chamber Humidity ● Oxygen content ● Print Layer Temperature
Impact
Moment-to-moment data will give an understanding to the impact on quality based on post process analysis.

Table 1.2: Research Question 2

Research Question 2	
How can each aspect's effect on each part quality metric be analyzed equally even though the metrics will have different scales, ranges, and units?	
Hypothesis 2.1	Hypothesis 2.2
A part must be designed that allows for a look at the change in build aspects versus the change in the part quality in order to compare the effects of the build aspects on the final quality of the part.	The oxygen content will show the largest relative change to part quality when compared with the changes from the humidity and the two temperature characteristics.
Methods	Methods
A tiered part will be designed that allows for the variable at hand to be changed to multiple levels thus providing a look at the change in part quality across multiple levels per print.	Post print analysis on part quality will be conducted to collect information on part quality which can be used to draw relationships to collected data.
Impact	Impact
An effective experiment design allows for the later analysis of part quality to be streamlined	A comparison between the part quality and the data collected during the experiment is required to develop the weighted calculation for the quality score.

Table 1.3: Research Question 3

Research Question 3
How can a robust quality score be calculated to provide a predictive view of part quality?
Hypothesis 3
The comparison made during the analysis must be used to weigh each aspect's in-situ value to calculate individual scores that combine into the overall score.
Methods
Use the discovered relationships to generate a quality score calculation that uses in-build data to predict part quality. <ul style="list-style-type: none"> ● Relative change in quality versus build characteristics ● Plotted data for the use of trendline equations
Impact
By using the gathered data and analyzed information the score can be made to predict the final quality during the print.

1.5 Thesis Format

The structure of the following work follows the previously shown outline with chapter 2 discussing the previous work in this area more in depth along with bridging the differences between the current and previous research. Chapter 3 details the methodology of the current work including experimental setup, experimental procedure, and finally how analysis was conducted. Chapter 4 covers the results and discussion. These chapters give insight into what the relationships found mean and go into the final development of the quality score along with how the robustness of the score was determined. Finally, chapter 5 reflects on the conclusions gathered from the conducted work. Along with these conclusions, avenues of research that the work can be taken are also discussed.

CHAPTER 2

LITERATURE REVIEW

A robust production quality is key to the implementation of metal additive manufacturing in industry. Currently, metal additive has a gap in the quality monitoring of parts as once a print has begun, the part quality must be analyzed after the part is finished. The inability for an engineer or operator to know if the part is within desired quality metrics prior to post print analysis makes this field lacking for industry use. This gap in application provides a research area for the creation of reliable methods of in-situ data monitoring for the use of predictive part quality.

2.1 Background Research

The field of data fusion lends itself to many applications. The industries that most commonly conduct research in this field include robotics, medical diagnostics, pattern recognition and many others (Varshney 2000). Research in data fusion previously covered the methodology of the fusion itself. The first methods for conducting the fusion of data were centralized and distributed data systems (Castanedo 2013). Centralized systems were optimal in the case that the cost of data transmission was zero and the computer resources needed were available. In this system the data is independent and normally distributed to the predicted value. The centralized method can introduce false measurements and be very computationally intensive when many aspects are tracked. These issues made the centralized method not as useful in a practical capacity thus for the most part distributed systems were used. Distributed systems come with other drawbacks such as the need for data alignment or the presence of out of sequence data measurements. This method however does work more practically in that it does not use the same unrealistic assumptions that centralized systems use. The work done by Hackett et al. provides a look at several more fields of data fusion and some challenges they face (Hackett 1990). Out of the several fields covered the most closely related to the proposed work was sensor modeling. There is one main issue that is often found when having multiple sensors collect data on a process. This sensor package often needs something to correct for errors or imprecise measurements collected during the process. This correction method can be as simple as using a logical sensor system. This system also helps with correctly aligning the data as the sensors may not all

collect data at the same interval. These aspects both need to be considered when designing the sensor package in the process as the data is both synced in the code and corrected using data analysis to determine data that is introduced because of the sensor and not the build itself. The integration of systems such as this can previously be seen in CNC machining operation to detect tool wear and other aspects regarding the subtractive process (Bray 1997). Integration through subtractive processes proved the usefulness of data fusion for use in industry as a method of process monitoring. This previous work provided both a good foundation for the field as well as a path forward for other researchers for the development of models for data collection in the comparatively more cutting-edge field of additive manufacturing. The potential issues one might face when conducting research in the field of additive production were yet to be discovered as the conceptual research had only implemented the actual use of either single or multiple sensors in subtractive processes. These problems were found when the research moved to using sensors in additive which initially involved using imaging sources to get layer-wise scans of the builds or parts.

2.2 Image Processing

The introduction of both plastic and metal additive manufacturing into industry allowed production to become more flexible in the parts and geometries produced. One of the drawbacks of both techniques is that the quality of the part is often a mystery during the actual build process. This is seen in the plastic field but is much more apparent in the metal additive field. Thus, there was larger industry interest for in-situ process monitoring using data fusion (Schmidt et al. 2017). The research in this field was needed by the additive manufacturing industry even just a small time ago in 2016 (Everton et al. 2016). By this time the need for a readily available method for implementing in-situ process monitoring was important and thus drove research in the field. At the time this was often done using one collection method or sensor type during the process.

The most common research done at the time involved the use of image processing to take layer-wise pictures or scans of the builds which can then be used to detect anomalies in the parts. The first research done involved the use of pictures of individual layers. This was often either done on each layer or only on

set sections of the part to attempt to detect process defects or anomalies. New work in this area expanded on using image processing by taking the scans instead of pictures of each layer and comparing the layer with the same layer in the CAD model to see the defects versus the ideal parameters (Lin et al. 2019; Kleszczynski). It can also be used in generating a 3D CAD model of the defect or anomaly which can then be used and analyzed on its own. Work has also been conducted using different imaging types such as thermal imaging. This is to not only get scans of the layers but also to gain insight through the thermal data of the builds (Esfahani ; Zeng ; Chivel and Smurov 2010). Thermal data is important to the additive manufacturing process and is especially important to metal additive processes (Raplee et al. 2017). This allows for more data to be considered for use in anomaly detection. A large problem in the advent of image processing was the method of handling all the images or data taken throughout the build. This issue allows a new section of research to be conducted to attempt to solve this problem.

The issue of data management was a large consideration when attempting to implement data collection and control to additive manufacturing. This gap in the understanding of data management research was initially resolved through the development of new models for handling the data gathered and the refinement of the methods used for data collection to improve anomaly detection (Sheykh Esmaili). The first models were centralized, and distributed models which either took data from many areas and joined them into a central system or took the data to several distributed servers. These methods were generalized methods and thus newer research needed more specific or robust methods of collection and organization. The prevalence of image collection drove a need for improvement on the models used to collect this data. Esfahani et al. developed a method to improve on the layer-wise image collection which was detailed as an auto-regressive image framing network (Esfahani). This network aid in the detection of anomalies by taking consecutive sets of thermal images. This set of images can be used to detect anomalies more effectively when compared to the previously used methods. This method also alleviated the issue of the previous methods which can only collect single images and thus gave local anomaly detection. The work done in the

image collection and processing field paved the way for more sophisticated methods which can analyze aspects simultaneously that cannot be seen using imaging alone.

2.3 Multi-Sensor Data Fusion Research

Recently, research in the field of in-situ quality monitoring of additive manufacturing has evolved to using multiple sensors to collect the data. These sets of multiple sensors can be a mix between the previous imaging techniques or solely several non-imaging data collection types. Non-imaging data collection includes temperature data, oxygen content, humidity data, or any other data that does not use an imaging source for collection. The non-imaging field has been a subject for research as it can allow for the determination of part qualities that image processes do not allow for. These aspects have been explored to gain an understanding of the relationship between the data the sensors can read versus the part parameters post-build. Research was done to discover the relationship of how build parameters can directly affect the part quality and the relationship of these to the other aspects of the process (Mani et al. 2015; Craeghs et al. 2010; Amado). A clear example of this is how the quality of a part in L-PBF or Directed-energy Deposition (DED) are dependent on the melt pool dynamics which is in turn related to the laser power; an example of this can be seen in Figure 2.1. The importance of determining part aspects such as porosity or surface roughness makes the monitoring of the related aspects vitally important to the improvement of the process (Zhang, Liu, and Shin 2019).

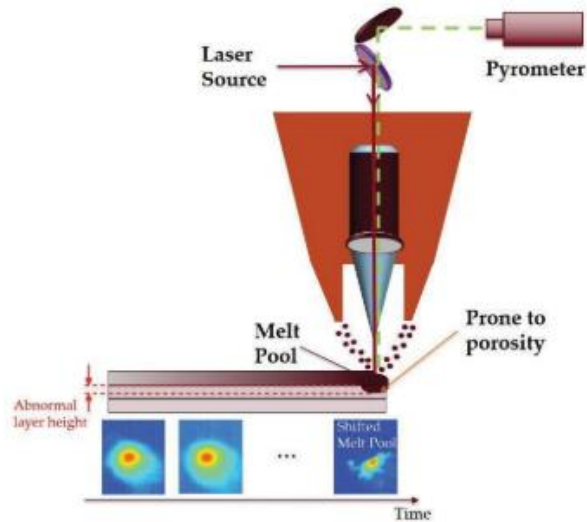


Figure 2.1: DED Melt Pool Dynamics

(Esfahani)

2.4 Machine Learning

Another aspect that was observed was that by controlling aspects such as build platform temperature the residual stresses in the build can be relieved and thus lends itself to being a controllable part parameter. Other researchers discussed the use of knowing the effects of melt pool dynamics on the part parameters in DED and PBF processes (Chua, Ahn, and Moon 2017; He, et al. 2019). A framework was proposed to use the relationship between the part quality and the melt pool dynamics. This framework consisted of a single layer, multi-layer, and final inspection. These inspections allow for a look at the part during the print. Laser cladding was also looked at for these types of relationships between part parameters and the data that can be monitored. For laser cladding, three aspects proved to be important which included part geometry, power density, and finally surface oxidation (Bi, Sun, and Gasser 2013). Many of the metal additive methods have issues with the same aspects however, L-PBF will not have as much of an issue with the oxidation as the chamber is a very low oxygen environment. By using this information on the relationship between part parameters and build parameters, researchers found that by controlling build parameters the process can be controlled. By combining this information with the in-situ part monitoring

this allows for the control of the part quality throughout the process. The research done in this field expanded from the previous image processing to systems of heterogeneous sensors to allow for more information about the current build. This information can be used in conjunction with each aspect's relationship to different part parameters to directly control part quality. Many researchers sought to improve on their data found in this field by improving the degree of process monitoring which was often done using machine learning.

Much of the research done both for imaging and multi-sensor data collection had one aspect in common in that many of them included the desire to branch into machine learning. By implementing machine learning the systems can be changed based on the previous data and learn to operate more effectively in the detection of process anomalies. Some research has already been done in this area both for image processing and multi-sensor systems. An expansion of work was seen in image processing by the addition of neural networks which can learn to detect processes (Zhang, Liu, and Shin 2019; Snow et al. 2021; Shevchik et al. 2019). Many of the research avenues of more recent times included putting the process monitoring of these systems online (Vandone, Baraldo, and Valente 2018; Rao et al. 2015). The transfer of the offline sensor data can be moved online to allow for constant process monitoring. Another way to implement the improvement of the process was to incorporate a feedback loop to the system. This loop allows the system to change based on the previous data taken. Another technique of machine learning was using the information available from the sensor package on the system to use data mining to attempt to improve the embedded feedback loop (Grasso). Researchers in the field of data fusion and monitoring of additive processes are still currently working on machine learning to allow for process improvement based on previous data points.

2.2 Presented Thesis Work

The goal of this work is to expand upon the past research in the field and integrate a single-novel score for quality control. The work is done specifically on the L-PBF process as comparatively few researchers have touched on this area when compared to the amount of research on DED or PBF. Exploration in the multi-sensor field was conducted and thus the use non-imaging systems to collect data

was chosen. The non-imaging collection method includes the development of a heterogeneous sensor package to include temperature sensors, oxygen content sensors, and chamber humidity sensors. Non-imaging was chosen because of the relative ease of acquiring sensors for the collection package as well as the gap in work of monitoring several build characteristics at once that is present currently. The sensor package includes many data streams to allow for information about the build to be collected and analyzed for the purposes of process monitoring. Data from this collection package was used to detect build anomalies or the onset of anomalies. The detection of build anomalies will allow the operator or engineer to stop a build based on the allowed criteria for the build. Allowed criteria, in this case, include the amount of surface roughness or porosity present in the part. By stopping the build early when the part is not within the desired range both time and material will be saved. Looking at multiple part quality characteristics, which is currently rarely done in the metal additive field, allows for a move to a holistic look at in-situ part quality. Another aspect of great interest is the development of a quality score calculation which allows the simplification of monitoring the process. Thus, the score allows operators or observers with less technical knowledge insight about the projected part quality. This score also is able to be subdivided to allow the engineer a detailed look about build aspects of the course of the print. The development of a score that simplifies quality while also allowing for a breakdown into individual data streams has not been done in the metal additive field. By allowing the engineer to view data over the course of the entire print, problems involved with the build can be diagnosed thus allowing for directed process improvement. The current work looks specifically at porosity and surface roughness with an additional goal to make the sensor package and quality score easily scalable. This allows the package and score to be changed to suit the needs of the process or engineering team.

CHAPTER 3

EXPERIMENTAL METHODS

Several experiments were conducted for the purpose of gathering quantitative data that were then compared to post print part data. This comparison provides the information that is the basis of the quality score. A large part of the setup of the experiment was determining how to collect the desired data and deciding what data should be collected.

3.1 Experimental Preparation

Prior to performing the experiment, several things needed to be determined with the most important of these being what data should be collected. The build aspects selected included chamber temperature, chamber humidity, print layer temperature, and finally chamber oxygen content. All these variables were changed and gathered during the experiment and thus allows insight into the relationships they have with the final part quality. Several of these variables are known to have a great impact on the L-PBF process such as oxygen content. (Wirth, et al.) The oxygen content in the chamber is a representation of how much argon is filling the chamber and thus how much shielding gas the process has and thus how protected the melt pool is from particulates. These main particulates in the L-PBF process are the soot coming off the melting process which can cause scattering of the laser. The print layer and chamber temperatures give insight into the effectiveness of the melting process at higher and lower temperatures. These temperatures effect the thermals of the surrounding area and at the plate which in addition to the thermal gradient of the laser change the part quality. A large presence of humidity in the chamber can cause the metal powder to clump and thus resulting in poor print quality. These aspects also were changed during the print either by the additive machine itself or through other means.

The first research question motivated the development of a multi-sensor data collection package. This multi-sensor data collection package was integrated to the machine and used to monitor all of the sensor data streams. This package was developed using an Arduino Uno microcomputer. This allows the sensor package to be run separately from the additive machine itself. A pictorial representation of how the sensor package, machine, and data collection computer can be seen in Figure 3.1.

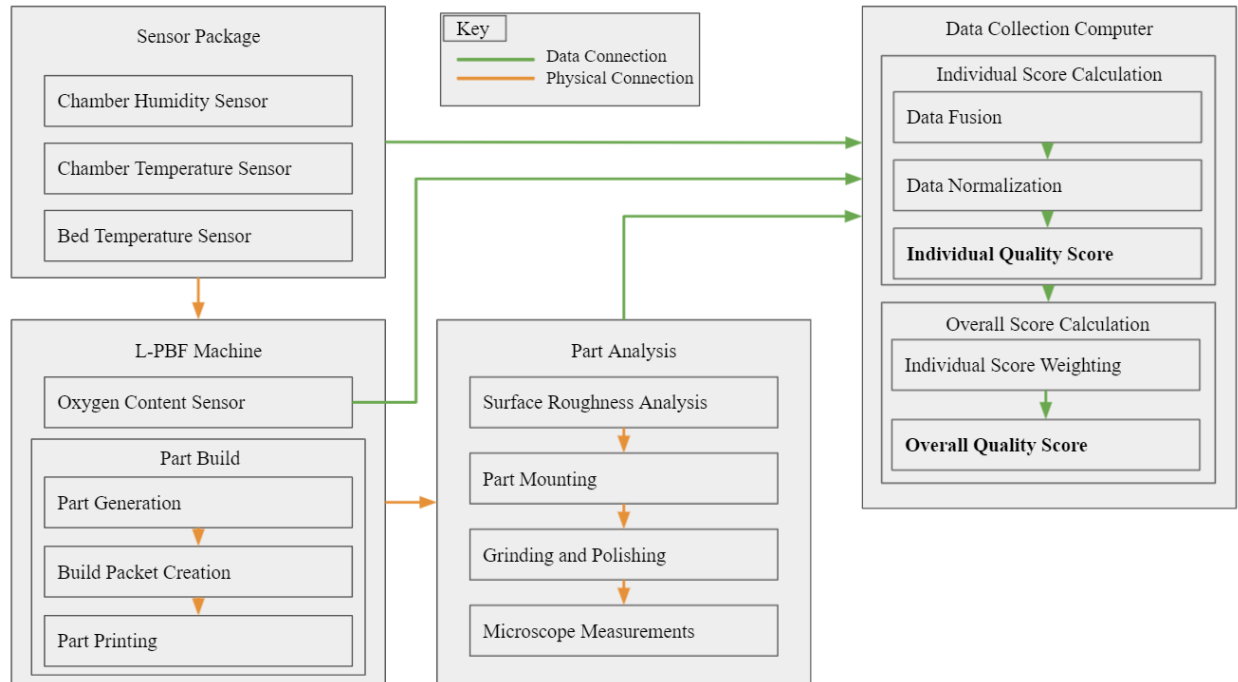


Figure 3.1: Relationship Schematic

The Arduino allows the package to be a self-contained item that directly transmits data to an external program for later analysis while also reducing the chance for the data stream to be interrupted because of any computer or software issues from the data collection computer. This package uses its own power supply to reduce the responsibility of the computer to just putting the collected data into an Excel file for later analysis and calculation of the quality score. A visual representation of the sensor can be found in Figure 3.2. The sensor from this package is integrated to the additive machine to record their specific data streams.



Figure 3.3: Experiment Part Design

The part design shown above reduces the overall printing by removing the need to each build aspect level to have a separate build. During the print the build aspect was modified to different values depending on the stage of the build. The tiered design of the part allows for clear separation of the different build aspect levels and thus allow each part to represent all three aspect levels. The vertical dimension was vitally important to the time the build takes as the X and Y movement of the machine is incredibly fast, but the Z movement is slowed because of the need to recoat more powder on the build volume. The height also was limited to no larger than 1.2in as any larger and the parts would not fit within the polishing molds. The height was set at 0.6in to allow for 0.1in of sacrificial supports to be added to reduce wasted material when the parts were cut from the build plate. The parts took 5.5 hours per print and as such the vertical height of the parts remained at a total of 0.6in.

Another concern that was addressed prior to the experiment was how to change build aspects during printing. Some of the aspects were changed by the additive machine such as the print layer temperature and oxygen content. The additive machine allowed for the print layer temperature to be fully automated. The L-PBF machine that was used for the experiments allowed the bed temperature to be changed according to the height that the build was at. Thus, the bed temperature was set to change at each of the notches between tiers. This in turn increases the temperature at the print layer. However, it was not a one-to-one change as

the farther along in the build the further the build plate heater was to the print layer and the more metal powder present to absorb the heat change. This did not present itself as a major issue as the values that were recorded by the sensor package can still be used to gain a comparison between print layer temperature and final part quality. The oxygen content was adjusted using the inert gas flow meters on the additive machine. By adjusting the inert gas flow valve the amount of argon gas input into the system was metered. The pressure inside the chamber remains constant because of the constant flow of gas leaving the machine. By adjusting the flow of the inert gas, the oxygen content was lowered during the print. This value was read by the additive machine and adjusted to the desired amount of oxygen per part section. The onboard software for the additive machine had records of the oxygen sensor values and this was going to be the source of the moment-to-moment data for analysis. The motivation behind this choice was that the oxygen sensor that the machine itself uses was much more precise and granular and it was thought that the records could easily be removed from the machine. This was not the case after the print; however, the oxygen was closely monitored and thus the oxygen content remained within $\pm 0.05\%$ of the desired values.

The chamber humidity and temperature were both very difficult to adjust as something needed to be added to the chamber to adjust these values. For the chamber humidity a dehumidifier was added into the chamber which can remove the already present humidity in the chamber, which was partially a product of the relative humidity in the room along with the humidity of the inert gas that was added to the chamber. The chamber temperature was adjusted using a heat gun which was set to produce as little airflow as possible to prevent any issues with the metal powder. Both appliances were almost impossible to adjust during the print without opening the chamber which would remove all the argon that was pumped in to remove the oxygen. In turn another Arduino based adjustment package was used to remove this issue. This Arduino was coded to take the sensor values from the data collection sensor package and use that information to turn a relay on and off which turns the power to the dehumidifier or the heat gun on and off according to the setpoint of the part tier. This setpoint was manually adjusted between each section of the print and thus this process was not entirely automated. A visual representation of the adjustment package setup can be seen in Figure 3.4.

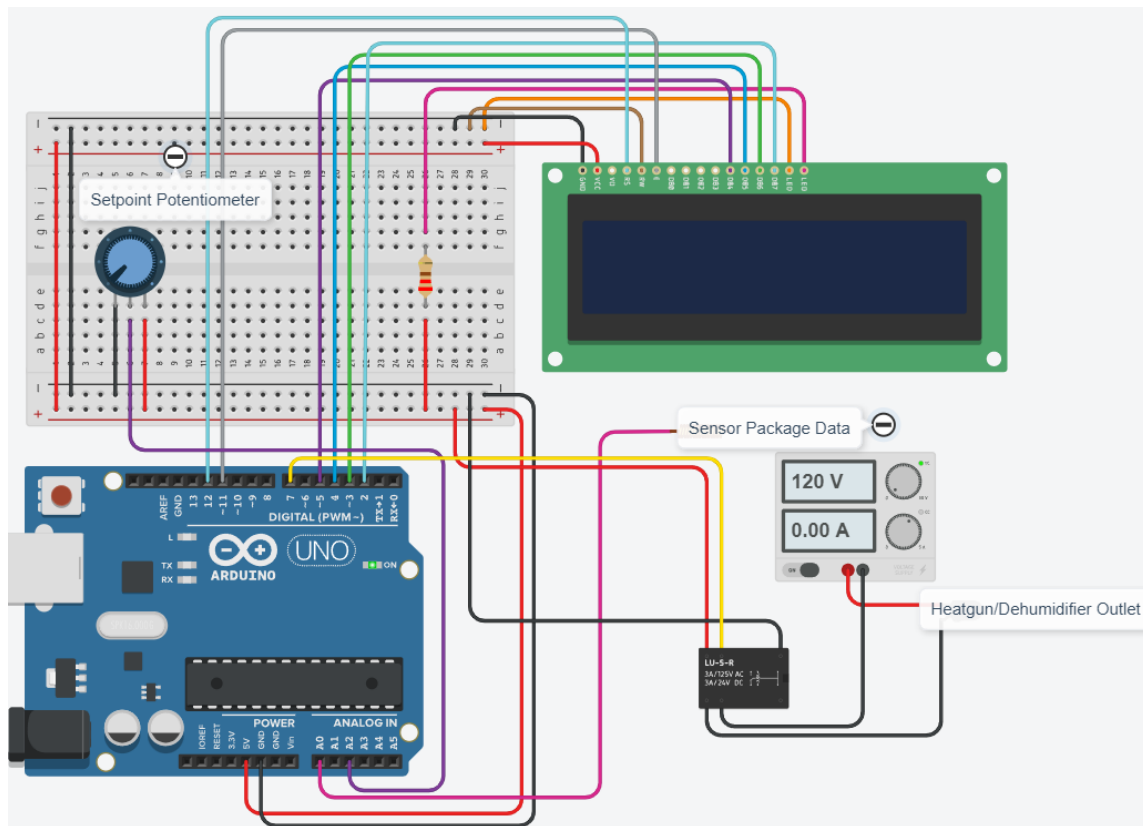


Figure 3.4: Adjustment Package

The code for the adjustment package takes the data from the main sensor package and compares the read value to a desired setpoint. This allows for a level to be set for an aspect and in turn determines if the current value was more or less than the desired setpoint. The aspect being monitored changes the requirement of being below or above the setpoint. In the case of the chamber temperature, the desired value is above the setpoint while the chamber humidity can be either above or below depending on the device used to change the humidity. This then sends a signal to a relay to turn on which in turn allowed the power to flow to the device used to raise or lower the build aspect. The package was used for a single aspect at a time and only for either chamber temperature or chamber humidity. While it only changes one aspect at a time the code and part of the wiring can be duplicated to allow for both chamber aspects to be read, set, and changed during the print.

3.2 Experimental Procedure

To gain insight to the relationship between the build aspects and the final part quality metrics an experiment was done for each build aspect. These experiments used the previously designed parts from Figure 3.3. The setup for the experiments included 30 of these parts along the middle of the build plate. A visual representation of the build setup can be seen in Figure 3.5. Each of the parts were oriented to one another so that no parts are blocking the recoating path of another part. This prevents a ripple effect that can often be seen when a part fails in front of another part thus damaging the recoater blade and causing subsequent parts in the path to fail. A gap of 0.1in was added between the build plate and the bottom of the part to add supports to reduce the amount of lost part material when cutting the parts off the build plate post print. The idea to use a total of 30 parts was done to make the statistical analysis more effective once all parts were printed.

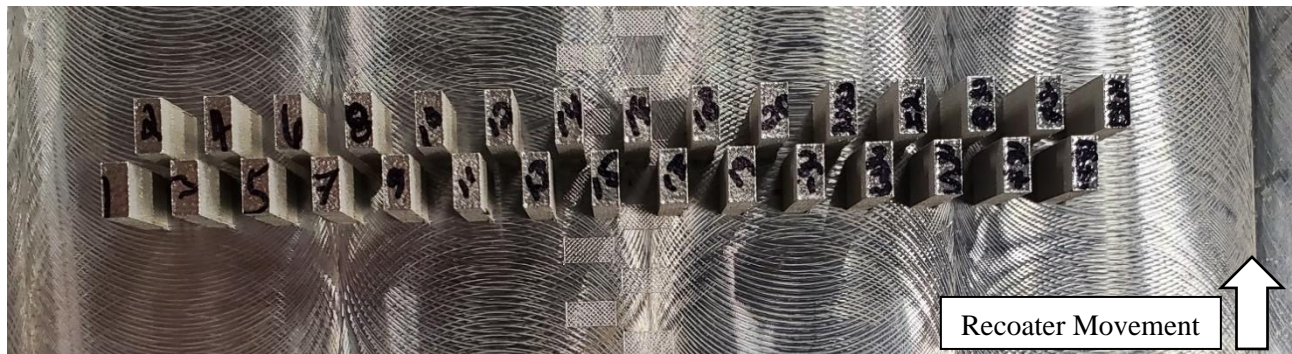


Figure 3.5: Build Setup

Once the build packet was designed and uploaded to the machine, the build aspect that was being changed during the experiment was adjusted to the point of its determined range that corresponded to the bottom section of the part. A table with all build aspect ranges can be seen in Table 3.1. These ranges are vital to comparing each characteristic's overall effect on part quality. Thus, these ranges are also vital to the determination of the largest contributors to part quality for both the surface roughness and porosity.

Table 3.1: Build Characteristic Ranges

Part Tier	Print Layer Temp	Chamber Temp	Chamber Hum	Oxygen Content
Units	°C	°C	%	%
Top	37.40	46.18	15.96	0.2
Middle	34.23	37.57	16.28	0.6
Bottom	29.66	26.89	16.38	1.00

Once the aspect was at the correct value for the first tier of the part, the print began. The amount of monitoring was different for each of the build aspects being observed. In the case of the oxygen content experiment the build had to be closely monitored to ensure that the tiers stayed close to their respective values. Once the oxygen was below 1.0% the amount of variability was greatly reduced and thus needed less intervention. This reduction in variability was an effect of the machine used for the experiment as it switches to a more precise sensor below 1.0% which increased the steadiness of the reading inside the chamber. The more precise oxygen sensor on the machine more finely controls the inlet and outlet valves and thus the same variability reduction effect was also seen on the sensor added to the machine by the sensor package.

Once the parts were finished printing, post print procedures were conducted starting with labeling the parts according to their position in the build volume and then to remove the parts from the build plate. The parts were labeled according to their position on the build plate for safety later during the analysis of the parts. Labeling the parts provides an explanation if several parts that had the same label showed skewed or outlier data. As an example, if all the parts labeled 3 for the four experiments showed information drastically different from the other 29 parts, then perhaps the location on the build plate changed these parts and this difference could be noted.

3.3 Part Analysis

Once the parts are separated from the build plate the final part quality was analyzed. The two-part quality metrics that were looked at were porosity and surface roughness across each of the part tiers. By

looking at these quality metrics across each of the part tiers, a relation between each build aspect and the final part quality metrics can be drawn. The importance of surface roughness to part quality is that for some applications a low surface roughness is required. Thus, parts that don't meet that requirement either get scrapped or go to post-processing to get to that required roughness. By monitoring the roughness and bringing the process to a point at which the roughness can be maintained below a certain level, less parts would need post-processing. The porosity of the part important to the determination of the final part quality along with the surface roughness. For parts made using metal additive, the porosity greatly affects the final determined part quality. Porosity is a measure of the number of voids and pores in a part and can either be its best when near zero, such as for the aerospace industry, or when inside a range that is above zero, such as for dental implants. Bland et al. stated that the most common way of improving the porosity is to increase the laser power to aid in the melting of powder. (Bland and Aboulkhair) However, the work that was conducted aimed to use non-imaging data streams on the build characteristics to improve both surface roughness and porosity. This allows for the changing of more than just the laser power to improve the porosity and thus gives more options to the process improvement.

The surface roughness of the tiers is found using a Keyence VR-3000 3D Macroscope. This measurement device allows for each part's non-notched surface to be scanned and then digitally post-processed which included leveling, cropping, and the removal of any anomalies that were not from the print itself. The macroscope was then used to acquire the average surface roughness (Sa) of each tier and then this data was exported to an Excel file for all 30 parts of each build aspect.

Finding the porosity required the middle of the parts to be viewable and thus requires more work than the surface roughness. This work was represented by the addition of polishing to gain access to the internal structure of the parts. Out of the total of 120 parts, 90 were mounted using MetLab quick set acrylic epoxy molding compound. Each part was unmolded after the 10-minute cure time was finished. The design of the parts put the total height well within the maximum 1.25in mold size. Once all parts were mounted in epoxy they were relabeled, separated, and organized to prevent any mixing of the different aspects. The polishing was done on a Pace Technologies NANO 1000T automatic grinder and polisher which can polish

up to six parts at a time. All parts went through several polishing steps which included 400 grit, 600 grit, 1200 grit, and finally 0.3-micron polishing. After polishing was completed each set of parts was analyzed using an Olympus BX35M microscope. While under the microscope the parts were recorded, seen in Figure 3.6, and scanned for porosity percentage across each tier. This was done by taking a line of pictures with one picture at each section. Keeping the pictures in the same line was done in an attempt to remove any user bias as the line of images were as strictly vertical as possible. This line was either relocated in the case of heavy anomalies such as many scratches or modified in the case of very few scratches. In the case of a light number of anomalies, such as one scratch on one section image, the line was deviated as little as possible to avoid said anomalies. These images were then analyzed using the on-board software to give a porosity percentage. These values were recorded along with the surface roughness in Excel.

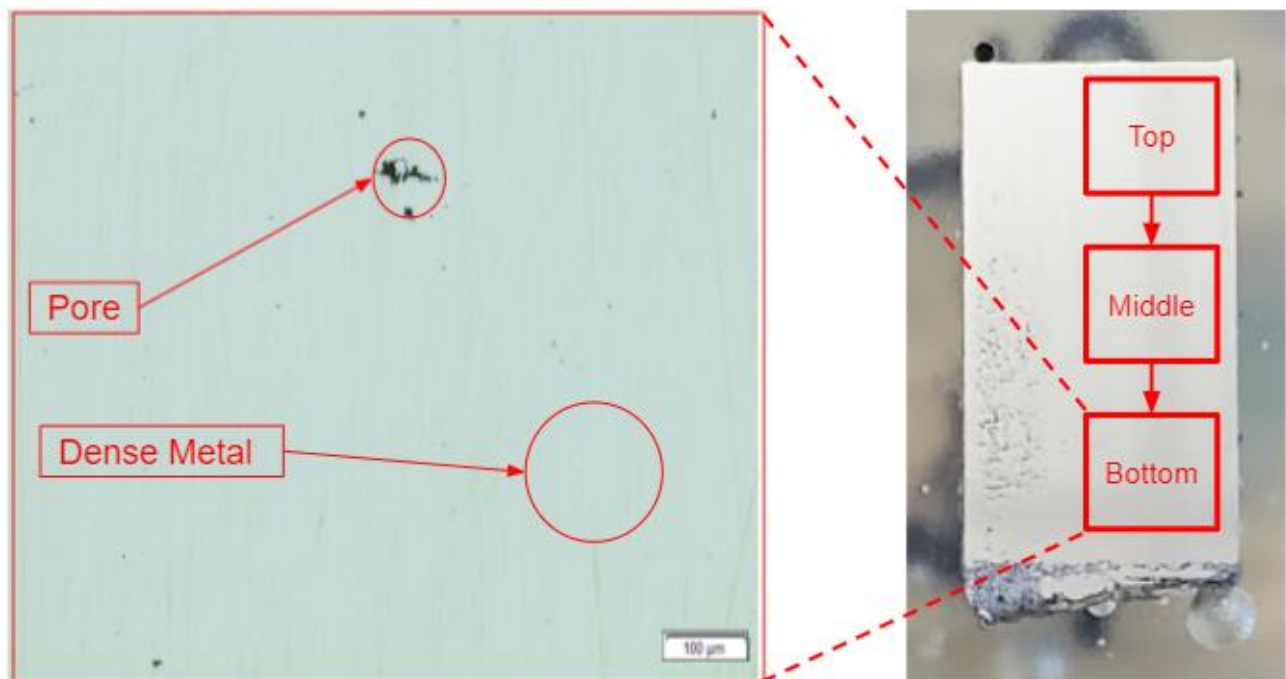


Figure 3.6: Porosity Collection Diagram

All the data gathered from both the macro and microscopes were used to numerically analyze the printed parts. The motivation when conducting the numerical analysis was to have a consistent comparison between all parts. This was done by observing the difference between each tier of the part for both build aspects and final part quality metrics, which in the case were the porosity and the surface roughness. By

looking at the amount of difference between tiers, in this case represented by a percentage change, the surface roughness and porosity can be compared even when the two have entirely different units. This also allows for a look at the largest contributors to quality given the design of the experiment would not investigate inter-characteristic relationships. All the printed parts in an aspect set were first looked at individually to determine if any outliers were present and, if present, the label on the outliers were marked to determine if any of the build plate positions were generating more outliers. After individually determining any relationships between position and outliers, each set of data was transformed for the calculation of the quality score. This was done by averaging the values for surface roughness and porosity at each section respectively. These values were plotted and a trendline was fit to the curve. This trendline gives the equation for each data set for both surface roughness and porosity which then was used in the quality score. These equations also were used to find a correlating value for the minimum and maximum part quality which were used to normalize the surface roughness and porosity quality scores prior to the total quality score.

3.4 Challenges Encountered

The largest challenges encountered included machine issues along with trouble developing both the sensor package and the adjustment package. The L-PBF machine used for the experiments had issues just before the experiments were conducted. This caused a large delay in the conducting of the work required for the final goal of the thesis. The main issue that caused the delay was the failure of the scanning system that moves the laser in the X and Y axis. This issue was not solved until a new scanner was installed which then allowed the thesis work to resume.

When beginning the work for this thesis it was known that an Arduino was a great route to take for creating the sensor package, but I had no experience in coding in any language at the time. This created the challenge of learning how to use and code for the Arduino microcomputers. By not have previous experience in coding, the development of both Arduino based packages took longer than expected. This, however, was resolved over the course of the thesis work as each step taken toward the final goal iterated the sensor package until the desired information can be gathered during the experiments. The adjustment

package was coded and assembled much more quickly as the development of the sensor package gave much needed practice and experience in both areas.

An issue was encountered during the experiment on the humidity's influence on part quality. When printing the parts, the expected humidity was assumed to be below the ambient humidity in the room but near that value. This, however, was not the case because the air in the room was already holding a large amount of moisture when compared to the argon gas that comprised the inert flow into the machine. The argon gas was dry when being pumped into the machine and thus rather than the expected humidity of 60% the actual humidity was 16%. This added an additional problem in that the already extremely low humidity of the gas made it very difficult to remove more humidity. This caused the range of the humidity data to be very small at just a change of 0.42% from bottom to top. The data for the humidity was still used because of the comparison between the change in characteristic and change in part quality. This caused an issue with the influence that the humidity had on the individual and overall quality scores. This was solved using normalization prior to the summing of all data streams into the individual scores.

CHAPTER 4

RESULTS & DISCUSSION

Post analysis data of the parts provided information about how each of the build characteristics affect the final part quality for surface roughness and porosity. This data also produces the equations required for the creation of the quality score.

4.1 Print Layer Temperature

From prior work the print layer temperature was expected to have a positive result on both aspects of the final part quality being observed. (Di Cataldo) The hypothesized result was that the increase in print layer temperature reduces the surface roughness and porosity thus improving final part quality. This was not the case for the print layer temperature once the printed parts were analyzed. The observed data showed two different cases for the surface roughness and the porosity.

The information collected from the surface roughness measurements showed that the print layer temperature saw a direct relationship with the surface roughness rather than the expected inverse relationship. As the print layer temperature was reduced from top to bottom the part saw a reduction in the overall surface roughness. This relationship can be seen graphically in Figure 4.1.

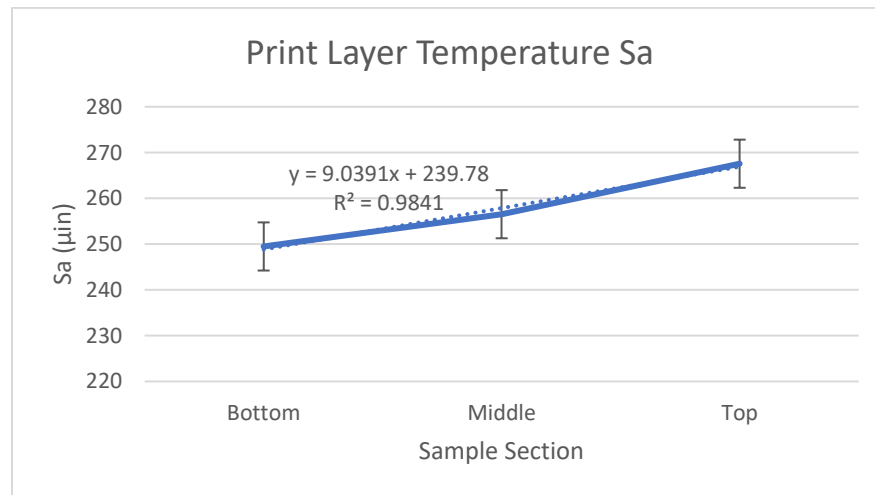


Figure 4.1: Print Layer Temperature Average Area Surface Roughness (Sa)

With this information, to get the desired best surface roughness, which for this case was the minimum surface roughness, the print layer temperature needed to be set at its lowest temperature of 100°C. The potential cause of the difference in the hypothesis and the actual data was that the increase in

temperature caused the powder to have less of a temperature differential from the laser. This causes the laser to melt the powder more easily, however this can also cause the laser to melt adjacent powder. The resulting surface roughness increases because of the laser melting powder outside of its controlled spot size which doesn't follow the same uniform melting pattern of the powder typically being melted.

The porosity showed a much different relationship to that of the surface roughness. In reference to the expected relationship, the print layer temperature followed closely to what was expected from prior work. As the print layer temperature was reduced from the bottom to the middle section and then from the middle to the top section, the porosity saw a decrease of 20.2% and 5.5% respectively. This relationship can be seen visually with Figure 4.2.

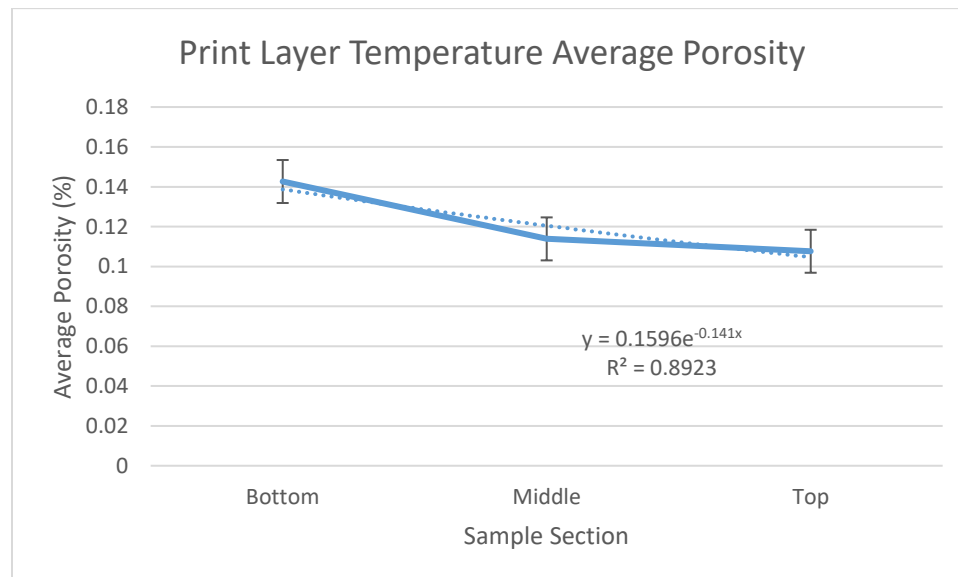


Figure 4.2: Print Layer Temperature Average Porosity (%)

As the increase in print layer temperature was conducted the porosity was expected to reduce which follows the results of the work. Parallels can be drawn from previous work done on the melt dynamics between the laser and powder. (Di Cataldo) The most important of these is that the less of a temperature differential between the laser and the powder the better the porosity can be. The lowered temperature differential caused the laser to more easily melt the powder which in the case of the porosity showed an improvement in part density and thus part quality. For the surface roughness the decrease in temperature

difference reduced the part quality by allowing the laser to melt adjacent powder which would not follow the same melt dynamics and thus produce a worse surface finish.

Both part quality metrics were plotted not only to get a visual representation of their relationship to the build characteristics but also to get a trendline for both surface roughness and porosity. The trend equations for these trendlines form the first part of the quality score for the print layer temperature. The surface roughness had a high R^2 value of 0.9841 with a linear trendline. This was different for the case of the porosity in that the linear trendline fit well but when an exponential trendline was introduced the fit was even better with a R^2 value of 0.8923. These trendlines were used to both find the minimum and maximum values for the print layer temperature while also allowing for incoming data to be transformed along both curves.

Table 4.1: Print Layer Temperature Averages

Print Layer Temp	Sa	Lower Section Change	Avg P	Lower Section Change
Units	μin	% Change	%	% Change
Top	267.561	4.30%	0.108	-5.45%
Middle	256.533		0.114	
Bottom	249.483	2.83%	0.143	-20.19%

4.2 Chamber Temperature

The expected results from the chamber temperature were that the behavior would be similar to the print layer temperature with the increase in heat allowing the laser to melt powder more easily. The chamber temperature showed an exceedingly different outcome to the print layer temperature. This however was not the case with this experiment. The largest difference between the two temperature readings was that the chamber temperature saw its worst and best quality in the middle section of the part. Alternatively, the print layer temperature saw the best and worst quality at either the top or bottom sections.

The surface roughness graph in Figure 4.3, shows this effect of the worst quality being in the middle section. The middle of the part saw a large increase in the surface roughness of 113.8% when moving from the bottom. When moving from the middle to the top section a decrease of 2.3% was seen in the surface roughness. This made the middle of the part the worst in terms of the surface roughness which when compared to the print layer temperature shows much different results.

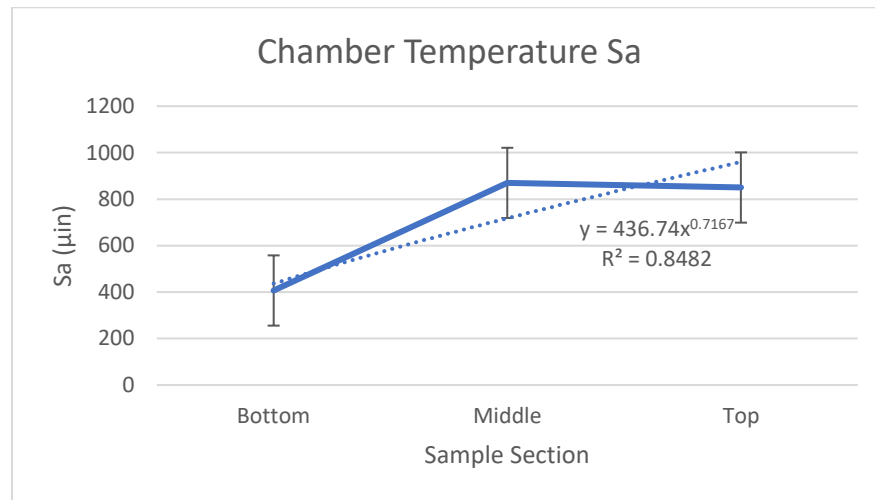


Figure 4.3: Chamber Temperature Average Area Surface Roughness (Sa)

More roughness reduction from middle to top might have been observed if not for an anomaly in the setup. As the temperature was increased using a heating source, the oxygen spiked momentarily. The spike in oxygen is attributed to one of two possible things. The first of these is that the heating source was heating the inert gas, in this case argon, and cause the oxygen left in the chamber to mix with the argon thus making the value read by the sensor to spike in oxygen because of the increase in oxygen around the sensor. The other cause that was theorized was that the heat changed the pressure of the gasses inside the chamber which again causes the gas to move contrary to the normal operation and thus tamper with the read value of the sensor causing the machine to input less inert gas than needed. This spike in oxygen was quickly reduced, but the parts saw a small amount of ridging which can be seen in Figure 4.4. In this figure, the red area along the bottom is the major ridging with the orange, yellow, and green areas representing the minor ridging.

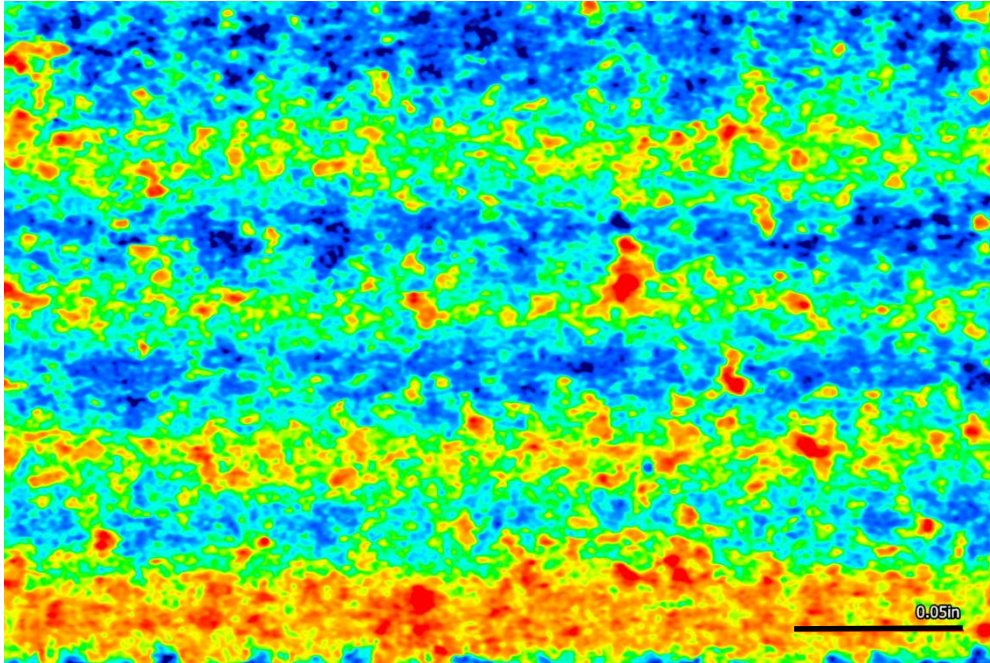


Figure 4.4: Chamber Temperature Sample 30 Top

This ridging was avoided as much as possible when taking the surface roughness which was easily done with the major ridging. The minor ridging was not as easily avoided as to remain consistent across all part in the experiment the worst of the minor ridging, which is seen as the primarily yellow region, had to be partially within the measured region. This issue might have had a minor effect on the value found for the surface roughness. The middle and bottom sections didn't have this issue and thus provide consistent data. Taking this issue into consideration while looking at Figure 4.3, the chamber temperature had a positive effect on the roughness outside of the middle block. The middle being worst of the part shows that for some of the build aspects there are sections of the range that produce the best part. This result was unexpected, however, when reflecting on this relationship it is logical as the build characteristic can provide improvement or deterioration up to a certain point. Once this point is crossed the part experiences a lower or higher part quality, respectively. Thus, for surface roughness, there is a worst value for the chamber temperature to be at which is near the average value of 37.57 °C. The chamber temperature was the largest contributor to the part quality in terms of the surface roughness. The increase of 113.8% moving from the bottom to the middle showed the largest change in the surface roughness across all data sets. This

information is strengthened by the fact that the middle and bottom sections were not affected by the ridging. The ridging, however, affected the overall surface roughness change from top to bottom and if not present the change from middle to top potentially saw a larger reduction in surface roughness. With this taken into consideration, the large change seen from middle to bottom allows the chamber temperature to remain as the largest contributor to surface roughness.

As was the case with the print layer temperature, the porosity provided the complete opposite results to the surface roughness. While the surface roughness saw its highest value at the middle section, the porosity showed its lowest value at the middle section. When the chamber temperature was reduced from the top to the middle section a reduction in porosity of 39.9% was seen. When moving from the middle to the bottom section the chamber temperature had an inverse effect on the part by raising the porosity by 75.5%. This drastic shift down and then back up in porosity can be seen in Figure 4.5.

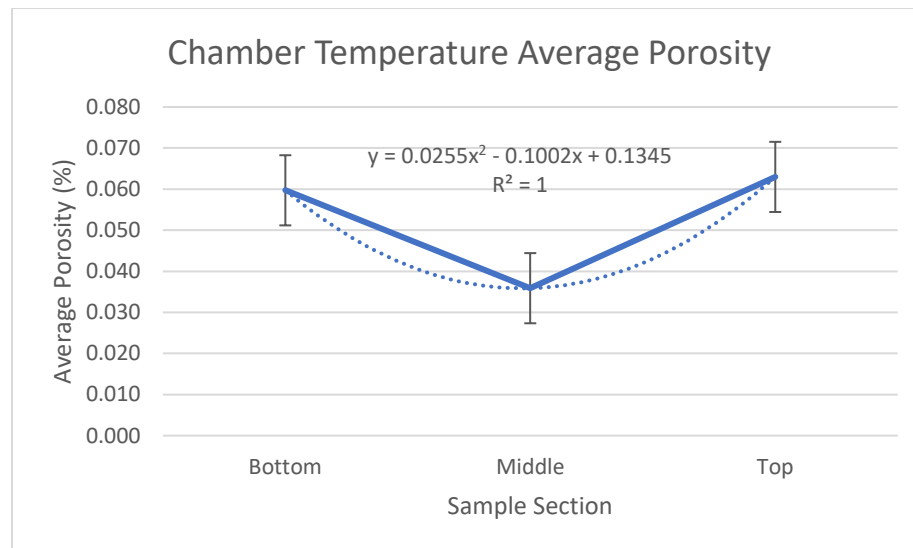


Figure 4.5: Chamber Temperature Average Porosity (%)

In the case of the surface roughness going below or above the middle range produces a part that is comparatively inferior to a part made within that range. For these parts the final part quality for surface roughness only saw a small reduction of 2.3% when moving above the observed worst area and when moving below the parts saw a large reduction in roughness of 113.8%. The porosity provided the complete inverse relationship than that of the surface roughness as the middle section had the best porosity

percentage. What this inverse relationship means is that to make the best part for surface roughness the chamber temperature must be outside of the best range for the porosity. By having the best surface roughness made outside of the range of the best porosity, there must be a decision made as to what factor is the most vital to the application.

The surface roughness showed its best fit with the power trendline. The R^2 value of 0.8482 shows that this trend is a good fit for the data present for the chamber temperature's surface roughness. The porosity had the trendline of a polynomial with order two. This trendline was more effective with more levels of the data set. By adding more sections than the three present, there would be more data points on the graph and thus more points to draw a trendline from. As the granularity of the part sections increase this trendline would be able to tell the function of the graphed data more accurately. This would also improve the robustness of the final quality score.

Table 4.2: Chamber Temperature Averages

Chamber Temp	Sa	Lower Section Change	Avg P	Lower Section Change
Units	μin	% Change	%	% Change
Top	850.085	-2.28%	0.063	75.47%
Middle	869.899		0.036	
Bottom	406.816	113.83%	0.060	-39.90%

4.3 Chamber Humidity

The chamber humidity was a very difficult characteristic to change, and this caused the range of the humidity to be relatively low. This, however, did not stop the humidity from influencing the final part quality. The hypothesized result for this characteristic was that as the humidity increased the degree of powder agglomeration and thus increase both the porosity and surface roughness. This primarily was not the case as the chamber temperature was changed.

The surface roughness saw a varied part quality across the three blocks similarly to the chamber temperature but with the best quality coming from the middle section. The graphed data can be seen in Figure 4.6. When observing the values for amount of increase and decrease in the part from section to section, the actual change was relatively small. From the top to the middle a 7.3% reduction in surface roughness was observed, while from the middle to the bottom an increase of 4.7% was present. This was a product of the small changes in the recorded humidity.

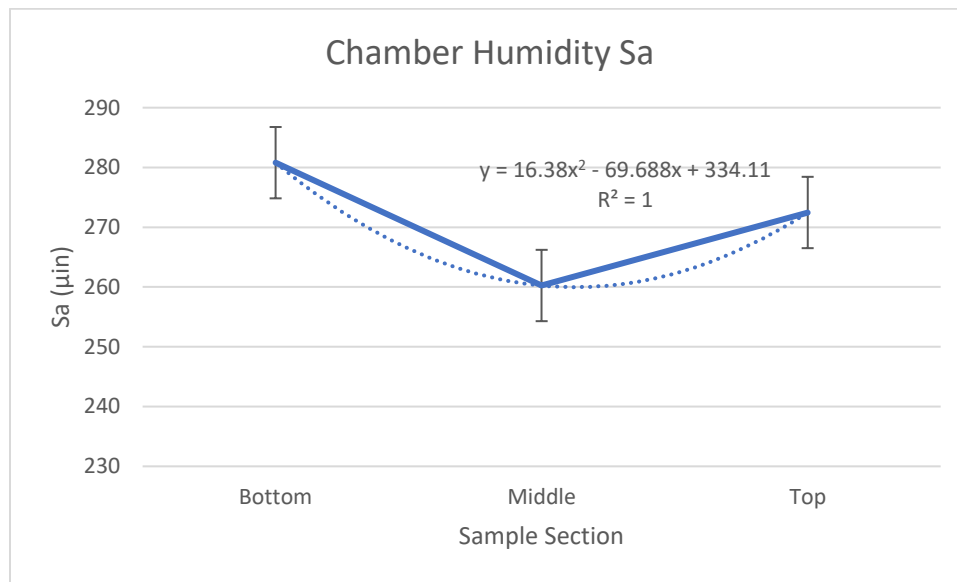


Figure 4.6: Chamber Humidity Average Area Surface Roughness (Sa)

The surface roughness saw the same effect that the chamber temperature's surface roughness experienced. This once again points to the concept of best ranges of the build characteristics. For the case of the humidity the observed best value for the surface roughness was to keep the humidity close to the 16.28% value that was present at the middle section of the part.

With the chamber temperature, the porosity showed an opposing graph that also had a best range. This, however, was not the case for the chamber humidity. The effects seen by the porosity were not seen in any other sample when observing the data for the humidity change. The main relationships seen from the other samples taken were either the presence of best ranges, such as for the chamber temperature, or a continued increase or decrease in the part quality such as what was seen in the print layer temperature's surface roughness data. The humidity had a different effect on the porosity which can be seen in Figure 4.7.

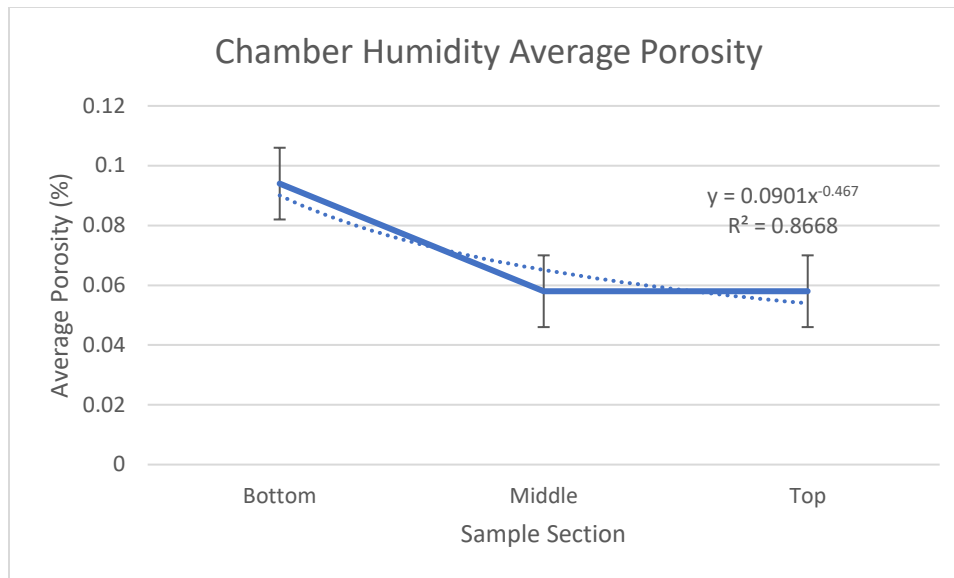


Figure 4.7: Chamber Humidity Average Porosity (%)

As the humidity was decreased between the bottom and middle sections of the parts a decrease of 38.3% in porosity was seen. This result was expected as with the reduction in humidity less agglomeration of adjacent powder particles would be present. The difference from all the other samples comes from the effect seen moving from the middle to the top sections. On average the middle and top sections had the same amount of porosity thus resulting in no percentage change in the two sections. With this information, the surface roughness and the porosity have a unique relationship to one another. The porosity having no reduction between the middle and top allows the best range for the surface roughness to also be best range for the porosity. This allows the build to be set at 16.28% humidity and get the best quality for both metrics without having to sacrifice one or the other. This effect wasn't seen in the previous two characteristics as with chamber temperature, both surface roughness and porosity had inversely prime areas for part quality. This introduces the choice of what to sacrifice to improve the part quality. The print layer temperature had a slightly different relationship between its part quality metrics. For that sample the surface roughness and porosity were linear and exponential, respectively, but they were also inverse to each other. Thus, when reducing the print layer temperature to reduce the surface roughness, the porosity gets exponentially worse. This relationship once again introduces a choice to the operation of the machine.

The trendline curves for both the surface roughness was an order two polynomial. This type of fit caters itself to the type of information gathered on the surface roughness and as the number of levels were increased the expectation is that this would remain the best fit. The porosity shows its best R^2 of 0.8668 with a power trendline. Logically this is a good fit as by moving bottom to middle a reduction is seen and then moving from middle to top a lesser change is seen which in this case was a change of 0%.

Table 4.3: Chamber Humidity Averages

Chamber Hum	Sa	Lower Section Change	Avg P	Lower Section Change
Units	μin	% Change	%	% Change
Top	272.467	4.69%	0.058	0.00%
Middle	260.253		0.058	
Bottom	280.799	-7.32%	0.094	-38.30%

4.4 Oxygen Content

Oxygen content was expected to have the largest effect on the part quality. More specifically, this effect was hypothesized to be a positive effect as the oxygen decreased. This was not seen in the experiment as for both surface roughness and porosity an inverse relationship was seen. The surface roughness saw a relatively small change when moving between sections. When moving from bottom to middle an increase of 1.9% was seen and a 3.6% increase was observed between the middle and top sections. This can be seen graphically in Figure 4.8. This relationship was the inverse of the expected results as instead of directly improving the surface roughness the oxygen content increased the surface roughness as it was decreased. The small increases in surface roughness as the oxygen increased point to the part being of higher quality when closer to the bottom section value of 1.0% oxygen in the chamber. The decrease to 0.2% interacted with the part by increasing the roughness along with the porosity.

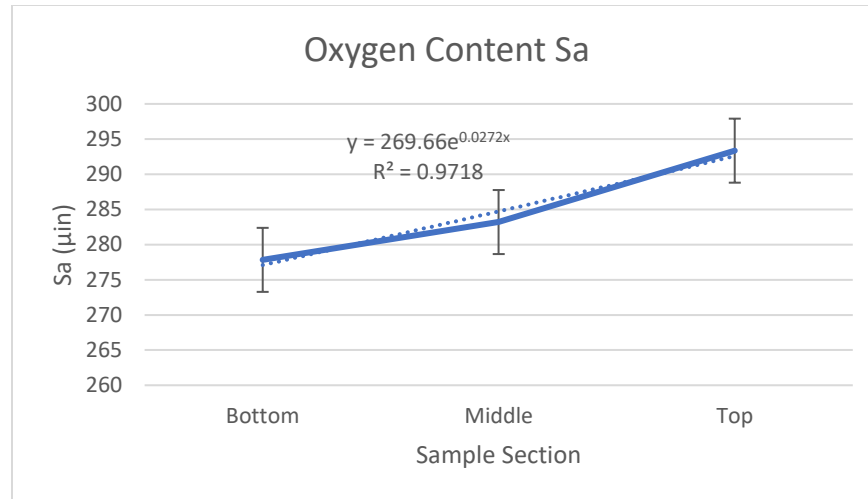


Figure 4.8: Oxygen Content Average Area Surface Roughness (Sa)

The porosity saw a very similar effect to the surface roughness. The differences in part quality were much larger than what was observed in the surface roughness. An increase of 17.1% was seen moving from the bottom to the middle block which is a normally sized increase when compared to other parts. The move from middle to top saw a sizeable increase of 148.5% which is the largest change seen in the collected data. This can be seen in the graphed data in Figure 4.9. Thus, while the expected result for the relationship was not seen, the expected largest contributor to part quality was confirmed to be oxygen at least in the case of the porosity. The largest contributor to the part quality in terms of surface roughness was the previously mentioned chamber temperature which, even with the issues stated about the ridging, beats all other samples.

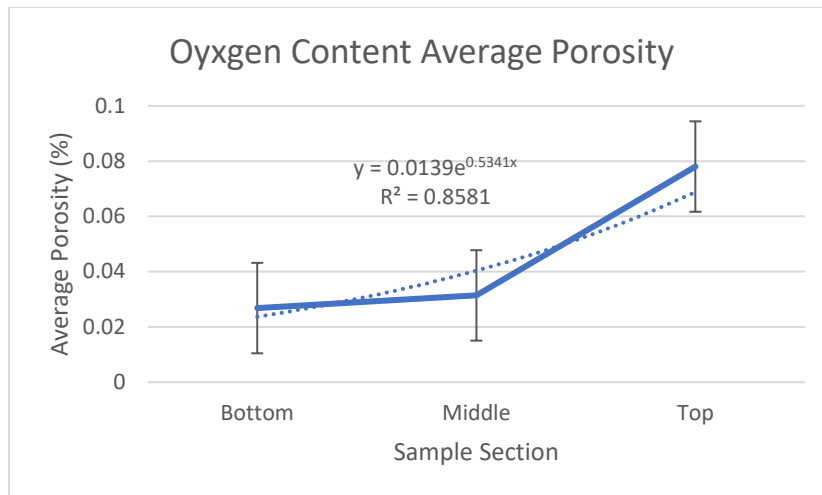


Figure 4.9: Oxygen Content Average Porosity (%)

There are several potential causes for the disparity in the expected and actual results. While the flow rate of inert gas was kept within a range of 1-2 liters per minute, the increase in flow rate as the inert gas was adjusted to remove the oxygen potentially affected the powder dynamics. The increase in flow rate may have introduced turbulence that influenced the powder. Another potential cause is that the parts were not perfectly polished. This did not affect the surface roughness as the part underwent no transformation when moving to be scanned for surface roughness measurements. A non-perfect polish was suspected and several of the part were checked again to verify the quality of parts. The only parts that showed a degree of scratching or anomalies were either already marked as outliers or the threshold for the measurement was set to not include the scratches.

The quality metrics saw very similar graph shapes once plotted, they, however, showed different types of graphs that fit the best. For the surface roughness the trendline had a R^2 values of 0.9718 when an exponential fit was used. This provided a logical view of this data as when reducing the oxygen, the data had an increase from the bottom to middle and then a larger increase when moving from the middle to top. For the case of the porosity, an exponential curve provided the best fit at a R^2 value of 0.8581. The trends present would be more accurately determined with more granular data. With an increase from the current three levels, the trends would have more points to be able to use and thus a more precisely determined trend could be seen.

Table 4.4: Oxygen Content Averages

Oxygen Content	Sa	Lower Section Change	Avg P	Lower Section Change
Top	293.351	3.58%	0.078	148.49%
Middle	283.204		0.031	
Bottom	277.828	1.94%	0.027	17.11%

4.5 Quality Score

The analysis of the parts raised several questions of what the best possible part would be for the purposes of the experiment. With the porosity there is of course full density as the best possible outcome for the part. Thus, the best quality part for porosity was the lowest amount of porosity with full dense or 0% porous being a perfect part. The surface roughness was more difficult to set a best quality part for. The cause of this was the fact that there is no possible part with zero roughness. Moving from the idea that no part will be perfectly smooth, a theoretical best part must be set. In the machining world, there are gold standards for as machined finishes. These standards have been made and recorded for the last 60 or more years. The field of metal additive has not had the same amount of time that the machining field has had to record this best surface finish or roughness. With that in mind, the best surface roughness for the development of this quality score was set at the lowest surface roughness value recorded for each data set. The lowest and highest surface roughness values were set as the quality markers for 100% and 0% respectively.

When calculating the quality score, the information gained from the plotting of the data and the fitting of the trendlines was of the most importance. By plotting the data, a value for the minimum and maximum part quality were set per data set. The trendlines provide the transforming equations that take the incoming data and change it into the quality score. This transformation is marked as the quality factor for a data set, an example of this for the print layer temperature can be seen in equation 4.1.

$$QF(SR)_{PT} = 9.0391(X_{PT}) + 239.78 \quad (4.1)$$

The variable of X_{PT} represents the in-situ data that are continually inserted into the equation during the print. This process was done for both the surface roughness and porosity for each data set. This equation is represented by the QF variable when moving to the surface roughness and porosity quality scores. Prior to moving to the part metric quality scores however, these scores were normalized across their minimum and maximum values. The justification behind the normalization was that the score needed to be put across a 0-100% range for readability. The normalization was introduced at this point in the calculation rather than later for several reasons. The first reason was that the design of the experiment did not allow for the inter-characteristic relationships, such as the effect between the print layer temperature and oxygen content on the surface roughness, to be determined. As such, the prior analysis was restricted to the individual level on the changes seen in the part. This allowed for the effect of one data set on the part quality to be observed but not the interaction between all the data sets. To get information on the largest contributors to quality, the part quality change versus the characteristic change was calculated which gave a relative concept of the comparative influence on part quality. The score itself then normalized and averaged the characteristics together because the determinations on the largest contributors was conducted prior to this point and did not need to be done again. The second reason was that when first calculating the score, a normalization was done on the final quality score. This allowed for the humidity data to vastly swing the score by a maximum of 50% and 75% in surface roughness and porosity respectively. This issue was introduced mainly due to the small change in the range of humidity. The change of 0.42% caused the initial calculation of the quality factor to be the most influential by far when that was not seen in the analysis of the data. This issue was first resolved with moving the normalization earlier in the calculation. When the score was moved from the first iteration that used the ratio of percent change in the quality versus the change in the characteristic to the current use of trendlines, this issue was eliminated but the point of normalization remained at the same

point. The motivation behind this was to improve the quality score by removing any issues, such as large changes to the score with little characteristic change, when expanding the score in the future.

Considering this, equation 4.2 shows the calculation of one of the two quality scores needed for the final quality score. This equation shows the collection of all the current four data sets while allowing for the expansion of the score by adding more sensors which increases the number of data sets. This equation was repeated for the porosity just as was conducted with the quality factor calculation. These individual scores allow for the final score to be broken down and observed individually if needed. This increased granularity of the score allows for a greater view of the part quality along with the ability to look closely at specific aspects that may be of interest.

$$QS(SR) = \frac{QF(SR)_{PT} + QF(SR)_{CT} + QF(SR)_{CH} + QF(SR)_{O_2} + \dots}{n} \quad (4.2)$$

The final step in the calculation of the quality score was to weight the individual scores and total them. Through the introduction of a weighting variable, denoted by W in equation 4.3, the individual scores to be joined together. Without weights, the score moves to a multi factor design which is a much more complex analysis of the part quality. This increase in complexity is the driving force for why so little research has been done on multiple part quality characteristics at once in metal additive. The addition of weights to the individual scores allows for the overall score to be made without implementing the multi factor design which would require an experimental design that observes the inter-characteristic relationships. With the surface roughness and porosity weights implemented into the overall score, the user of the score can tailor the desired result to their process. This proves useful in different applications that may require a move towards full density without the need for the best surface roughness possible. This score is similarly left open to the introduction of new part quality metrics outside of the surface roughness and porosity, such as the internal stresses.

$$QS(Total) = (W(SR) * QS(SR)) + (W(P) * QS(P)) + \dots \quad (4.3)$$

CHAPTER 5

CONCLUSIONS

In conclusion, the creation of a predictive quality score for the L-PBF process was the desired goal of this work. This score introduces a predicative element to the metal additive quality control field. This score was produced through the creation of an experiment that allowed for a build characteristic to be changed during the print. This provides a look at several characteristics' relationships to quality and the score in allows for several ambient aspects of the print to be considered at once. The current work in this field mainly observes the melt dynamics through thermal imaging or one build aspect's relation to quality at a time. Two separate quality metrics provide the basis of the quality score that was calculated using the trends found by plotting the data from the prints.

The key takeaways were that the chamber temperature was the largest contributor to the surface roughness. This result was unexpected and resulting from this a look at any issues introduced during the print was done. During the last section of the chamber temperature print a small amount of ridging was introduced which was thought to be the cause comparatively unusual chamber gas dynamics introduced by the increase in temperature. The largest contributor to the quality of the porosity was the oxygen which was the expected result. However, the oxygen negatively affected the porosity which was first assumed to be a positive characteristic. This difference was investigated and was caused by either the inert flow corrupting the powder dynamics or the introduction of scratches to the polished parts. Both issues were avoided as much as possible by having a low change in the flow rate in the case of the inert flow deviating the powder dynamics and by adjusting the threshold for the scanning to avoid possible scratches. Once the parts were analyzed a score for each quality metric was calculated and normalized across a 0-100% scale.

There are several areas of expansion for this work in the future. The first of these would be a reassessment of the design for the experiment. The experiment could be redesigned in two ways, through the implementation of statistical methods or through the addition of more data levels. Through the implementation of a statistics-based design of experiments, the inter-characteristic relationships can be found. This would also allow for the addition of more analysis in the form of multiple regressions.

Following a regression analysis, the statistical equations found could be optimized and implemented to increase the robustness of the quality score. This would also allow for the implementation of machine learning software to the quality score. The other aspect of the experiment that would be changed is the addition of more levels of the build characteristics. By increasing the number of levels from the current three, the best fit equations would have more data points to draw from and thus more accurate. The increase in best fit accuracy would increase the accuracy of the quality score. Moving past the proposed improvements to the experiment, another way to expand on this work would be the implementation of cloud-based data management. By having the sensor package and quality score connected to an online server, the score could be seen anywhere that can access the internet. This would allow for the quality to be viewed even when not present at the machine thus increasing the useability of the score. This online aspect could also serve as a database of previous data and thus allow for past prints to be viewed and analyzed.

REFERENCES

(Amado ; Bi, Sun, and Gasser 2013; Bland and Aboulkhair 2015; Bleiholder and Naumann 2009; Bray ; Castanedo 2013; Chivel and Smurov 2010; Chua, Ahn, and Moon 2017; Craeghs, et al. 2010; Di Cataldo 2021; Esfahani ; Everton, et al. 2016; Grasso ; Hackett 1990; He, et al. 2019; Hu, Chen, and Zhou 2013; John 2019; Kleszczynski ; Lehmhus et al. 2016; Li, et al. 2019; Lin, et al. 2019; Mani, et al. 2015; Montazeri et al. 2019; Ning et al. 2019; Rao ; Rao, et al. 2015; Raplee, et al. 2017; Schmidt, et al. 2017; Sekhar ; Shevchik, et al. 2019; Sheykh Esmaili ; Snow, et al. 2021; Vandone, Baraldo, and Valente 2018; Varshney ; Wirth, et al. 2021; Zeng ; Zhang, Liu, and Shin 2019)

Amado, Antonio. "Advances in SIs Powder Characterization."

Bi, G., C. N. Sun, and A. Gasser. 2013. "Study on Influential Factors for Process Monitoring and Control in Laser Aided Additive Manufacturing." *Journal of Materials Processing Technology* 213, no. 3: 463-468. <https://dx.doi.org/10.1016/j.jmatprotec.2012.10.006>.

Bland, Stewart, and Nesma T. Aboulkhair. 2015. "Reducing Porosity in Additive Manufacturing." *Metal Powder Report* 70, no. 2: 79-81. <https://dx.doi.org/10.1016/j.mprp.2015.01.002>.

Bleiholder, Jens, and Felix Naumann. 2009. "Data Fusion." *ACM Computing Surveys* 41, no. 1: 1-41. <https://dx.doi.org/10.1145/1456650.1456651>.

Bray, Olin. 1997. "Data Fusion for Adaptive Control in Manufacturing."

Bray, Olin H. "<Data Fusion for Adaptive Control.Pdf>."

Castanedo, F. 2013. "A Review of Data Fusion Techniques." *ScientificWorldJournal* 2013: 704504. <https://dx.doi.org/10.1155/2013/704504>.

Chivel, Yu, and I. Smurov. 2010. "On-Line Temperature Monitoring in Selective Laser Sintering/Melting." *Physics Procedia* 5: 515-521. <https://dx.doi.org/10.1016/j.phpro.2010.08.079>.

Chua, Zhong Yang, Il Hyuk Ahn, and Seung Ki Moon. 2017. "Process Monitoring and Inspection Systems in Metal Additive Manufacturing: Status and Applications." *International Journal of Precision Engineering and Manufacturing-Green Technology* 4, no. 2: 235-245. <https://dx.doi.org/10.1007/s40684-017-0029-7>.

Craeghs, Tom, Florian Bechmann, Sebastian Berumen, and Jean-Pierre Kruth. 2010. "Feedback Control of Layerwise Laser Melting Using Optical Sensors." *Physics Procedia* 5: 505-514. <https://dx.doi.org/10.1016/j.phpro.2010.08.078>.

Di Cataldo, Santa. 2021.

"<Optimizing_Quality_Inspection_and_Control_in_Powder_Bed_Metal_Additive_Manufacturin

[g_Challenges_and_Research_Directions.Pdf>." https://dx.doi.org/10.1109/JPROC.2021.3054628.](https://dx.doi.org/10.1109/JPROC.2021.3054628)

- Esfahani, Mehrnaz Noroozi. "In-Situ Layer-Wise Quality Monitoring for Laser-Based Additive Manufacturing Using Image Series Analysis."
- Everton, Sarah K., Matthias Hirsch, Petros Stravroulakis, Richard K. Leach, and Adam T. Clare. 2016. "Review of in-Situ Process Monitoring and in-Situ Metrology for Metal Additive Manufacturing." *Materials & Design* 95: 431-445. [https://dx.doi.org/10.1016/j.matdes.2016.01.099.](https://dx.doi.org/10.1016/j.matdes.2016.01.099)
- Grasso, Marco. "Data Fusion Methods for Statistical Process Monitoring and Quality Characterization in Metal Additive Manufacturing."
- Hackett, Jay. 1990. "Multi-Sensor Fusion: A Perspective."
- He, Wei, Wenxiong Shi, Jiaqiang Li, and Huimin Xie. 2019. "In-Situ Monitoring and Deformation Characterization by Optical Techniques; Part I: Laser-Aided Direct Metal Deposition for Additive Manufacturing." *Optics and Lasers in Engineering* 122: 74-88. [https://dx.doi.org/10.1016/j.optlaseng.2019.05.020.](https://dx.doi.org/10.1016/j.optlaseng.2019.05.020)
- Hu, Ju Rong, Long Chen, and Jing Zhou. 2013. "Multifunction Simulator for Radar Test." *Applied Mechanics and Materials* 278-280: 893-896. [https://dx.doi.org/10.4028/www.scientific.net/AMM.278-280.893.](https://dx.doi.org/10.4028/www.scientific.net/AMM.278-280.893)
- John, Klaess. 2019. "3 Definitions of Quality in Manufacturing and Why They Matter." Form of Item. [https://tulip.co/blog/definition-of-quality-4-0/.](https://tulip.co/blog/definition-of-quality-4-0/)
- Johnson, Kristen. 2001. "Philip B Crosby's Mark on Quality."
- Juran, Joseph; Godfrey, A Blanton. 1998. "Juran Quality Handbook."
- Kleszczynski, Stefan. "Error Detection in Laser Beam Melting Systems by High Resolution Imaging."
- Lehmhus, Dirk, Claus Aumund-Kopp, Frank Petzoldt, Dirk Godlinski, Arne Haberkorn, Volker Zöllmer, and Matthias Busse. 2016. "Customized Smartness: A Survey on Links between Additive Manufacturing and Sensor Integration." *Procedia Technology* 26: 284-301. [https://dx.doi.org/10.1016/j.protcy.2016.08.038.](https://dx.doi.org/10.1016/j.protcy.2016.08.038)
- Li, Zhixiong, Ziyang Zhang, Junchuan Shi, and Dazhong Wu. 2019. "Prediction of Surface Roughness in Extrusion-Based Additive Manufacturing with Machine Learning." *Robotics and Computer-Integrated Manufacturing* 57: 488-495. [https://dx.doi.org/10.1016/j.rcim.2019.01.004.](https://dx.doi.org/10.1016/j.rcim.2019.01.004)

- Lin, Weiyi, Hongyao Shen, Jianzhong Fu, and Senyang Wu. 2019. "Online Quality Monitoring in Material Extrusion Additive Manufacturing Processes Based on Laser Scanning Technology." *Precision Engineering* 60: 76-84. <https://dx.doi.org/10.1016/j.precisioneng.2019.06.004>.
- Mani, Mahesh, Brandon Lane, Alkan Donmez, Shaw Feng, Shawn Moylan, and Ronnie Fesperman. 2015. <https://dx.doi.org/10.6028/nist.Ir.8036>.
- Montazeri, Mohammad, Abdalla R. Nassar, Christopher B. Stutzman, and Prahalada Rao. 2019. "Heterogeneous Sensor-Based Condition Monitoring in Directed Energy Deposition." *Additive Manufacturing* 30. <https://dx.doi.org/10.1016/j.addma.2019.100916>.
- Ning, Jinqiang, Daniel E. Sievers, Hamid Garmestani, and Steven Y. Liang. 2019. "Analytical Modeling of Transient Temperature in Powder Feed Metal Additive Manufacturing During Heating and Cooling Stages." *Applied Physics A* 125, no. 8. <https://dx.doi.org/10.1007/s00339-019-2782-7>.
- Rao, Prahalad K. "<Sensor Based Fault Detection.Pdf>."
- Rao, Prahalad K., Jia Liu, David Roberson, Zhenyu Kong, and Christopher Williams. 2015. "Online Real-Time Quality Monitoring in Additive Manufacturing Processes Using Heterogeneous Sensors." *Journal of Manufacturing Science and Engineering* 137, no. 6. <https://dx.doi.org/10.1115/1.4029823>.
- Raplee, J., A. Plotkowski, M. M. Kirka, R. Dinwiddie, A. Okello, R. R. Dehoff, and S. S. Babu. 2017. "Thermographic Microstructure Monitoring in Electron Beam Additive Manufacturing." *Sci Rep* 7 (Mar 3): 43554. <https://dx.doi.org/10.1038/srep43554>.
- Schmidt, Michael, Marion Merklein, David Bourell, Dimitri Dimitrov, Tino Hausotte, Konrad Wegener, Ludger Overmeyer, Frank Vollertsen, and Gideon N. Levy. 2017. "Laser Based Additive Manufacturing in Industry and Academia." *CIRP Annals* 66, no. 2: 561-583. <https://dx.doi.org/10.1016/j.cirp.2017.05.011>.
- Sekhar, Ravi. "<Tripathi_Humiditymetaladditive.Pdf>."
- Shevchik, Sergey A., Giulio Masinelli, Christoph Kenel, Christian Leinenbach, and Kilian Wasmer. 2019. "Deep Learning for in Situ and Real-Time Quality Monitoring in Additive Manufacturing Using Acoustic Emission." *IEEE Transactions on Industrial Informatics* 15, no. 9: 5194-5203. <https://dx.doi.org/10.1109/tii.2019.2910524>.
- Sheykh Esmaili, Kyumars. "<Data Stream Processing in Complex Applications.Pdf>." <https://dx.doi.org/10.3929/ethz-a-006689762>.
- Snow, Zackary, Brett Diehl, Edward W. Reutzler, and Abdalla Nassar. 2021. "Toward in-Situ Flaw Detection in Laser Powder Bed Fusion Additive Manufacturing through Layerwise Imagery and

Machine Learning." *Journal of Manufacturing Systems* 59: 12-26.
<https://dx.doi.org/10.1016/j.jmsy.2021.01.008>.

Vandone, Ambra, Stefano Baraldo, and Anna Valente. 2018. "Multisensor Data Fusion for Additive Manufacturing Process Control." *IEEE Robotics and Automation Letters* 3, no. 4: 3279-3284.
<https://dx.doi.org/10.1109/lra.2018.2851792>.

Varshney, P. K. "<Multisensor_Data_Fusion_Varshney.Pdf>."

Varshney, P.K. 2000. "Multisensor Data Fusion."

Wirth, Florian, Alex Frauchiger, Kai Gutknecht, and Michael Cloots. 2021. "Influence of the Inert Gas Flow on the Laser Powder Bed Fusion (Lpbf) Process." In *Industrializing Additive Manufacturing*, 192-204.

Zeng, Kai. "A Review of Thermal Analysis Methods in Laser Sintering and Selective Laser Melting."

Zhang, Bin, Shunyu Liu, and Yung C. Shin. 2019. "In-Process Monitoring of Porosity During Laser Additive Manufacturing Process." *Additive Manufacturing* 28: 497-505.
<https://dx.doi.org/10.1016/j.addma.2019.05.030>.

APPENDIX A
PRINT LAYER TEMPERATURE DATA

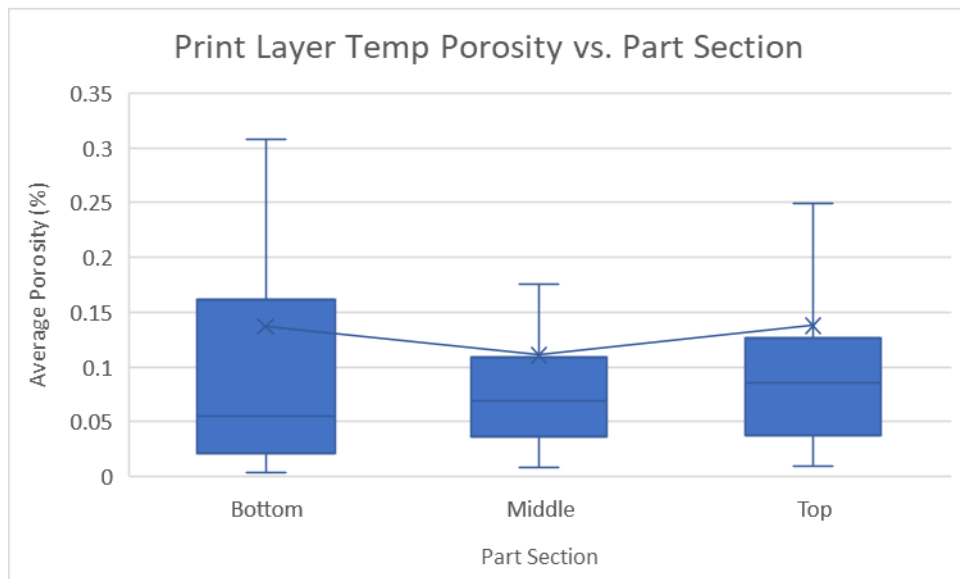
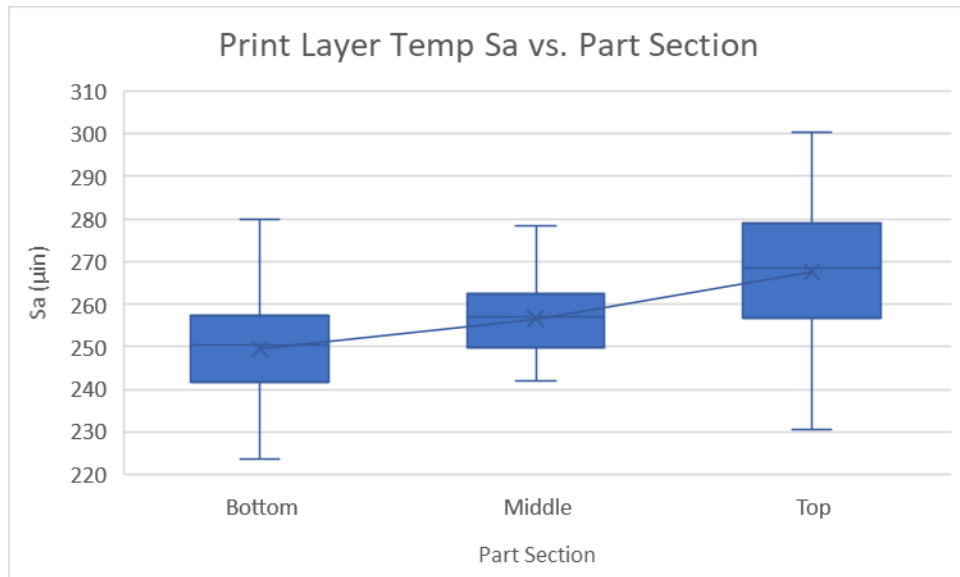
Print Layer Temperature	Sa (μin)			Avg Porosity (%)		
Part	Top	Middle	Bottom	Top	Middle	Bottom
1	264.72	257.77	255.34	0.07	0.04	0.31
2	254.96	241.84	244.54	0.12	0.36	0.53
3	257.36	255.44	260.11	0.52	0.46	0.62
4	268.67	255.75	255.01	0.18	0.18	0.15
5	272.64	259.54	246.89	0.04	0.04	0.09
6	269.37	314.25	253.84	0.06	0.11	0.16
7	274.31	256.97	248.16	0.08	0.06	0.15
8	283.73	257.41	263.30	0.03	0.10	0.05
9	288.70	270.55	279.96	0.25	0.30	0.27
10	258.21	248.53	244.32	0.01	0.08	0.06
11	276.87	256.12	259.25	0.10	0.09	0.02
12	275.37	256.76	254.60	0.01	0.03	0.02
13	265.14	256.97	238.23	0.09	0.02	0.03
14	246.06	250.08	232.20	0.04	0.04	0.16
15	264.63	243.69	233.21	0.11	0.01	0.01
16	287.00	262.17	258.23	0.13	0.08	0.05
17	240.93	229.56	223.64	0.06	0.05	0.02
18	281.09	259.23	261.93	0.12	0.02	0.00
19	300.44	278.28	242.49	0.02	0.10	0.04
20	285.38	277.59	250.54	0.71	0.05	0.02
21	253.91	242.65	238.66			
22	278.24	268.50	252.39			
23	276.76	264.73	248.66			
24	268.46	255.60	258.78			
25	294.10	253.50	250.20			
26	258.74	259.24	249.50			
27	230.66	218.10	231.08			
28	262.47	263.50	256.83			
29	243.41	228.73	237.14			
30	244.49	252.97	255.46			

APPENDIX B
PRINT LAYER TEMPERATURE STATISTICS

Print Layer Temperature					
Surface Roughness					
<i>Top</i>		<i>Middle</i>		<i>Bottom</i>	
Mean	267.561	Mean	256.533	Mean	249.483
Standard Error	3.052	Standard Error	3.115	Standard Error	2.126
Median	268.568	Median	256.866	Median	250.369
Mode	#N/A	Mode	#N/A	Mode	#N/A
Standard Deviation	16.719	Standard Deviation	17.062	Standard Deviation	11.643
Sample Variance	279.518	Sample Variance	291.125	Sample Variance	135.549
Kurtosis	-0.339	Kurtosis	4.175	Kurtosis	0.685
Skewness	-0.203	Skewness	0.824	Skewness	-0.011
Range	69.778	Range	96.149	Range	56.318
Minimum	230.662	Minimum	218.100	Minimum	223.641
Maximum	300.440	Maximum	314.249	Maximum	279.960
Sum	8026.830	Sum	7696.004	Sum	7484.482
Count	30	Count	30	Count	30
Confidence Level(95.0%)	6.243	Confidence Level(95.0%)	6.371	Confidence Level(95.0%)	4.347
Porosity					
<i>Top</i>		<i>Middle</i>		<i>Bottom</i>	
Mean	0.138	Mean	0.111	Mean	0.137
Standard Error	0.039	Standard Error	0.028	Standard Error	0.038
Median	0.085	Median	0.069	Median	0.055
Mode	#N/A	Mode	#N/A	Mode	#N/A
Standard Deviation	0.176	Standard Deviation	0.124	Standard Deviation	0.172
Sample Variance	0.031	Sample Variance	0.015	Sample Variance	0.030
Kurtosis	6.195	Kurtosis	3.033	Kurtosis	2.923
Skewness	2.511	Skewness	1.932	Skewness	1.849
Range	0.699	Range	0.454	Range	0.612
Minimum	0.010	Minimum	0.009	Minimum	0.004
Maximum	0.708	Maximum	0.463	Maximum	0.616
Sum	2.753	Sum	2.213	Sum	2.733
Count	20	Count	20	Count	20
Confidence Level(95.0%)	0.082	Confidence Level(95.0%)	0.058	Confidence Level(95.0%)	0.081

APPENDIX C

PRINT LAYER TEMPERATURE BOX PLOTS



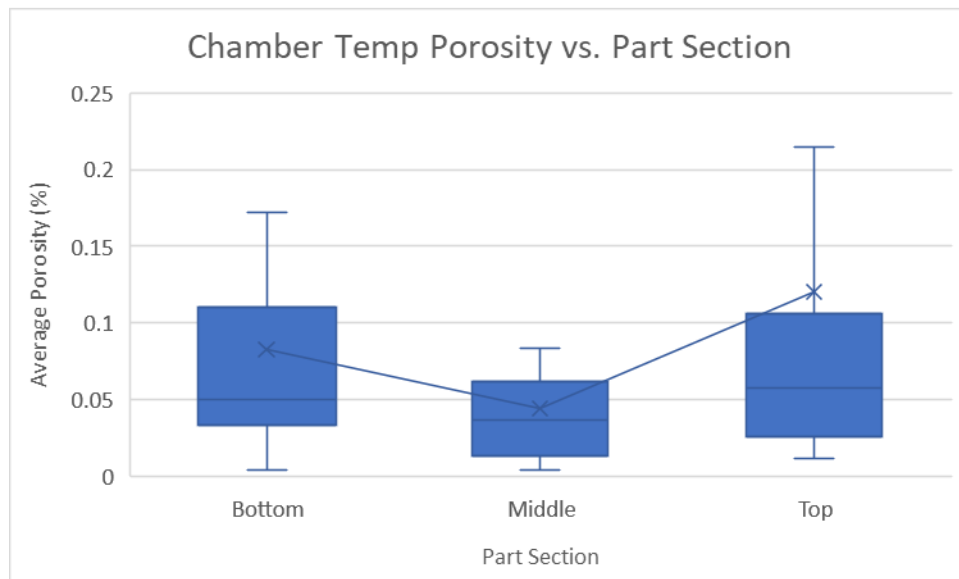
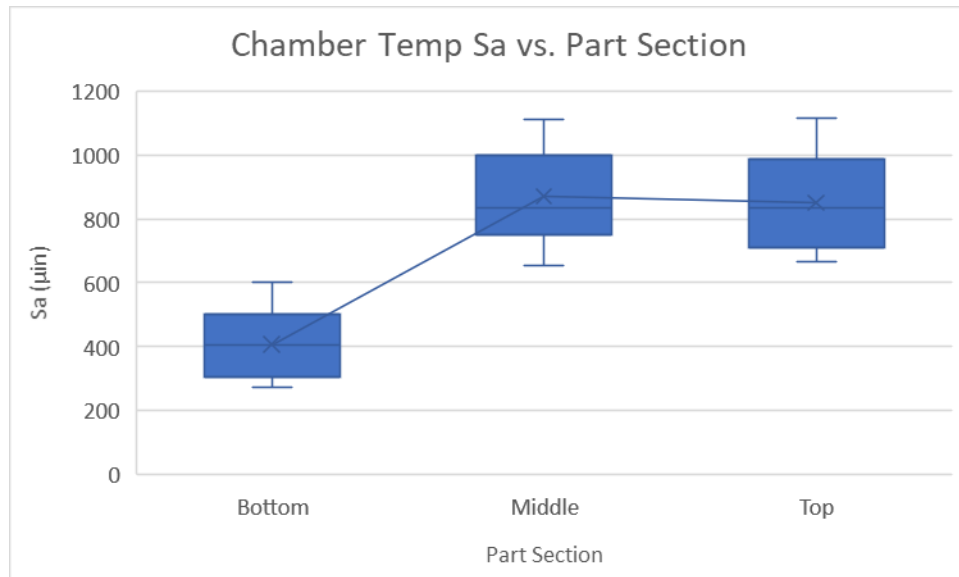
APPENDIX D
CHAMBER TEMPERATURE DATA

Chamber Temperature Part	Sa (μin)			Avg Porosity (%)		
	Top	Middle	Bottom	Top	Middle	Bottom
1	1114.73	1105.19	602.54	0.04	0.06	0.11
2	1073.00	1083.76	559.39	0.16	0.06	0.05
3	1055.32	1079.98	557.39	0.10	0.04	0.04
4	1028.56	1109.60	569.85	0.05	0.03	0.07
5	1040.53	1059.32	532.44	0.02	0.01	0.05
6	990.62	1026.95	499.44	0.11	0.02	0.01
7	985.71	1025.86	520.28	0.04	0.03	0.30
8	1030.59	990.72	514.67	0.08	0.02	0.02
9	956.83	937.31	466.13	0.13	0.07	0.17
10	910.15	953.92	442.55	0.08	0.04	0.04
11	934.81	981.92	453.15	0.02	0.06	0.16
12	900.99	945.23	420.09	1.08	0.06	0.24
13	878.16	910.31	454.79	0.01	0.01	0.04
14	841.14	818.66	400.75	0.02	0.05	0.08
15	876.67	836.16	409.14	0.21	0.18	0.10
16	816.63	864.51	420.19	0.03	0.00	0.05
17	829.46	808.32	361.54	0.04	0.01	0.03
18	736.88	811.73	367.09	0.03	0.01	0.01
19	742.52	833.66	361.91	0.07	0.04	0.00
20	786.05	809.42	355.11	0.10	0.08	0.07
21	748.29	767.88	300.68			
22	700.17	782.56	307.18			
23	716.91	760.92	313.34			
24	663.94	724.26	290.35			
25	692.79	698.86	305.11			
26	708.06	703.95	281.42			
27	682.73	671.93	277.79			
28	707.47	655.29	277.22			
29	687.81	667.43	309.06			
30	665.07	671.35	273.87			

APPENDIX E
CHAMBER TEMPERATURE STATISTICS

Chamber Temperature					
Surface Roughness					
	<i>Top</i>	<i>Middle</i>		<i>Bottom</i>	
Mean	850.085	Mean	869.899	Mean	406.816
Standard Error	26.176	Standard Error	26.763	Standard Error	18.812
Median	835.299	Median	834.915	Median	404.945
Mode	#N/A	Mode	#N/A	Mode	#N/A
Standard Deviation	143.374	Standard Deviation	146.586	Standard Deviation	103.040
Sample Variance	20556.039	Sample Variance	21487.436	Sample Variance	10617.248
Kurtosis	-1.330	Kurtosis	-1.253	Kurtosis	-1.193
Skewness	0.289	Skewness	0.171	Skewness	0.309
Range	450.791	Range	454.314	Range	328.669
Minimum	663.942	Minimum	655.288	Minimum	273.874
Maximum	1114.733	Maximum	1109.602	Maximum	602.543
Sum	25502.552	Sum	26096.973	Sum	12204.479
Count	30	Count	30	Count	30
Confidence Level(95.0%)	53.537	Confidence Level(95.0%)	54.736	Confidence Level(95.0%)	38.476
Porosity					
	<i>Top</i>	<i>Middle</i>		<i>Bottom</i>	
Mean	0.120	Mean	0.044	Mean	0.083
Standard Error	0.052	Standard Error	0.009	Standard Error	0.017
Median	0.057	Median	0.037	Median	0.050
Mode	#N/A	Mode	#N/A	Mode	#N/A
Standard Deviation	0.232	Standard Deviation	0.040	Standard Deviation	0.078
Sample Variance	0.054	Sample Variance	0.002	Sample Variance	0.006
Kurtosis	17.604	Kurtosis	6.237	Kurtosis	1.978
Skewness	4.100	Skewness	2.090	Skewness	1.550
Range	1.069	Range	0.174	Range	0.291
Minimum	0.012	Minimum	0.004	Minimum	0.004
Maximum	1.080	Maximum	0.178	Maximum	0.296
Sum	2.406	Sum	0.883	Sum	1.652
Count	20	Count	20	Count	20
Confidence Level(95.0%)	0.109	Confidence Level(95.0%)	0.019	Confidence Level(95.0%)	0.037

APPENDIX F
PRINT LAYER TEMPERATURE BOX PLOTS



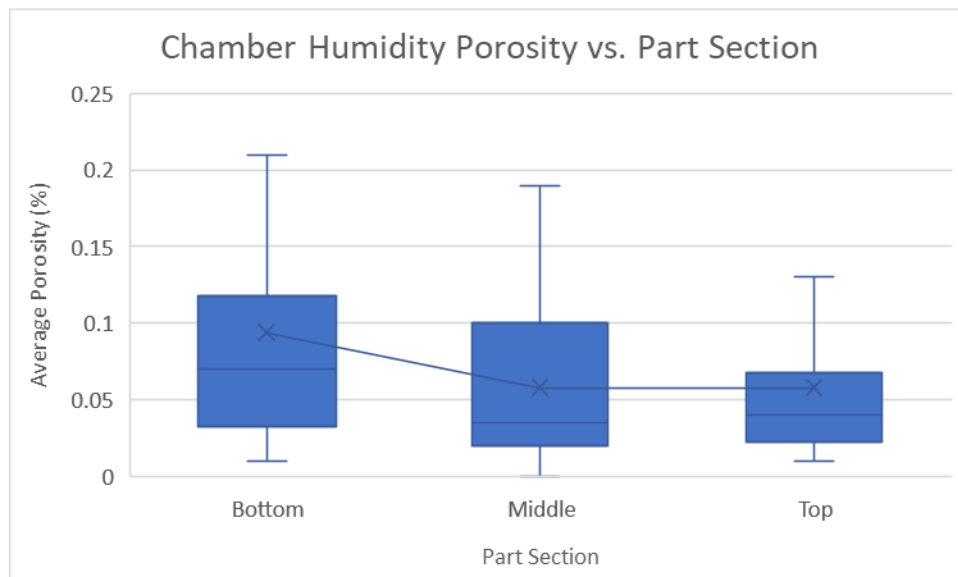
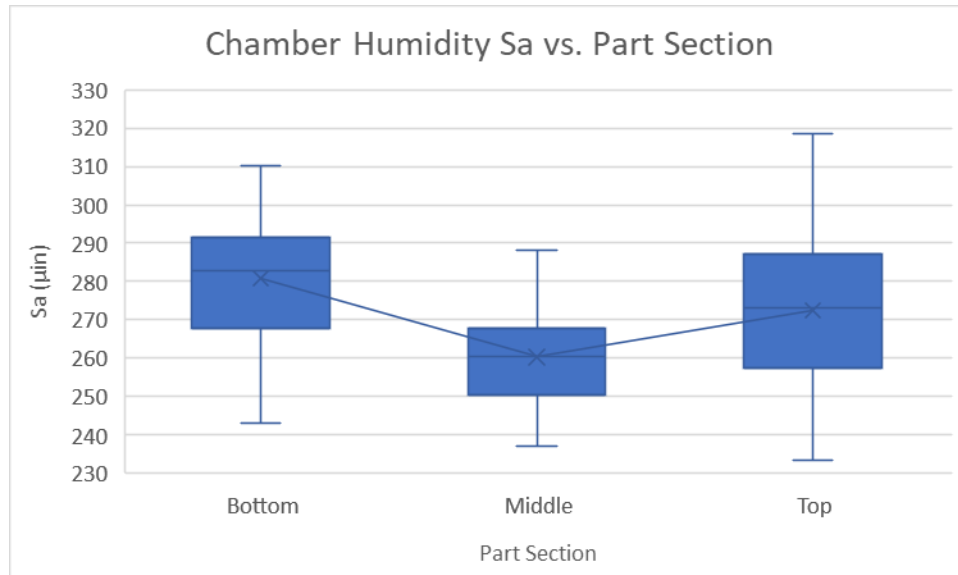
APPENDIX G
CHAMBER HUMIDITY DATA

Chamber Humidity Part	Sa (μin)			Avg Porosity (%)		
	Top	Middle	Bottom	Top	Middle	Bottom
1	301.96	275.98	303.48	0.13	0.12	0.10
2	257.97	253.63	291.98	0.18	0.03	0.07
3	287.84	283.21	310.05	0.06	0.06	0.06
4	277.10	262.88	308.01	0.17	0.19	0.10
5	263.02	258.20	289.29	0.04	0.11	0.12
6	253.80	250.87	289.36	0.02	0.07	0.21
7	272.00	266.65	298.89	0.05	0.07	0.20
8	255.37	254.23	293.33	0.10	0.02	0.02
9	253.28	252.11	299.36	0.06	0.17	0.33
10	257.90	267.03	290.25	0.04	0.03	0.07
11	272.95	266.96	286.93	0.06	0.00	0.01
12	273.78	263.95	291.54	0.03	0.12	0.03
13	318.45	280.69	288.31	0.01	0.02	0.06
14	249.17	247.03	267.90	0.07	0.05	0.17
15	287.74	274.62	275.27	0.03	0.02	0.11
16	296.67	275.49	286.98	0.01	0.01	0.08
17	244.59	242.37	257.28	0.04	0.04	0.02
18	286.73	266.59	281.97	0.01	0.02	0.04
19	311.75	288.23	278.52	0.03	0.00	0.02
20	289.72	270.19	283.87	0.02	0.01	0.06
21	279.49	248.62	277.50			
22	273.83	262.05	277.92			
23	284.34	258.50	278.26			
24	265.59	256.34	264.57			
25	276.63	266.04	276.35			
26	254.31	240.99	252.23			
27	273.39	242.60	260.15			
28	260.72	251.81	254.61			
29	260.64	242.60	266.73			
30	233.29	237.12	243.08			

APPENDIX H
CHAMBER HUMIDITY STATISTICS

Chamber Humidity					
Surface Roughness					
<i>Top</i>		<i>Middle</i>		<i>Bottom</i>	
Mean	272.467	Mean	260.253	Mean	280.799
Standard Error	3.612	Standard Error	2.452	Standard Error	3.065
Median	273.170	Median	260.275	Median	282.920
Mode	#N/A	Mode	242.600	Mode	#N/A
Standard Deviation	19.782	Standard Deviation	13.428	Standard Deviation	16.785
Sample Variance	391.308	Sample Variance	180.316	Sample Variance	281.744
Kurtosis	0.003	Kurtosis	-0.687	Kurtosis	-0.326
Skewness	0.408	Skewness	0.193	Skewness	-0.387
Range	85.160	Range	51.110	Range	66.970
Minimum	233.290	Minimum	237.120	Minimum	243.080
Maximum	318.450	Maximum	288.230	Maximum	310.050
Sum	8174.020	Sum	7807.580	Sum	8423.970
Count	30	Count	30	Count	30
Confidence Level(95.0%)	7.387	Confidence Level(95.0%)	5.014	Confidence Level(95.0%)	6.268
Porosity					
<i>Top</i>		<i>Middle</i>		<i>Bottom</i>	
Mean	0.058	Mean	0.058	Mean	0.094
Standard Error	0.011	Standard Error	0.013	Standard Error	0.018
Median	0.040	Median	0.035	Median	0.070
Mode	0.060	Mode	0.020	Mode	0.060
Standard Deviation	0.050	Standard Deviation	0.056	Standard Deviation	0.080
Sample Variance	0.003	Sample Variance	0.003	Sample Variance	0.006
Kurtosis	1.398	Kurtosis	0.415	Kurtosis	2.742
Skewness	1.461	Skewness	1.143	Skewness	1.580
Range	0.170	Range	0.190	Range	0.320
Minimum	0.010	Minimum	0.000	Minimum	0.010
Maximum	0.180	Maximum	0.190	Maximum	0.330
Sum	1.160	Sum	1.160	Sum	1.880
Count	20	Count	20	Count	20
Confidence Level(95.0%)	0.023	Confidence Level(95.0%)	0.026	Confidence Level(95.0%)	0.038

APPENDIX I
CHAMBER HUMIDITY BOX PLOTS



APPENDIX J
OXYGEN CONTENT DATA

Oxygen Content Part	Sa (μin)			Avg Porosity (%)		
	Top	Middle	Bottom	Top	Middle	Bottom
1	316.86	288.41	276.28	0.12	0.01	0.03
2	279.26	256.51	295.17	0.05	0.02	0.03
3	287.86	285.84	312.12	0.05	0.02	0.01
4	333.35	322.20	323.79	0.09	0.03	0.03
5	303.31	280.20	291.64	0.06	0.02	0.02
6	325.37	312.04	290.05	0.02	0.01	0.03
7	293.20	290.78	291.16	0.04	0.02	0.01
8	462.00	299.37	291.11	0.05	0.02	0.03
9	295.79	302.25	287.46	0.08	0.04	0.01
10	273.86	268.00	258.58	0.02	0.01	0.07
11	289.71	298.58	298.16	0.04	0.05	0.01
12	307.12	293.78	274.98	0.05	0.05	0.02
13	281.03	279.39	278.87	0.22	0.03	0.01
14	283.30	283.12	277.66	0.04	0.05	0.02
15	285.79	299.35	271.92	0.37	0.77	2.25
16	308.53	287.13	307.32	0.03	0.05	0.04
17	259.68	262.67	284.03	0.23	0.04	0.06
18	299.51	303.19	299.33	0.24	0.06	0.01
19	304.44	296.66	271.05	0.05	0.05	0.00
20	305.21	292.15	283.78	0.00	0.03	0.06
21	274.07	258.29	246.91			
22	313.98	309.68	266.39			
23	295.27	294.45	280.15			
24	283.77	261.85	259.98			
25	316.13	292.88	288.42			
26	291.41	273.45	259.73			
27	278.73	252.67	249.16			
28	278.69	252.21	248.48			
29	280.81	266.27	242.67			
30	261.13	248.95	241.77			

APPENDIX K
OXYGEN CONTENT STATISTICS

Oxygen Content					
Surface Roughness					
<i>Top</i>		<i>Middle</i>		<i>Bottom</i>	
Mean	298.973	Mean	283.743	Mean	278.270
Standard Error	6.486	Standard Error	3.585	Standard Error	3.824
Median	292.303	Median	287.772	Median	279.506
Mode	#N/A	Mode	#N/A	Mode	#N/A
Standard Deviation	35.527	Standard Deviation	19.634	Standard Deviation	20.945
Sample Variance	1262.178	Sample Variance	385.490	Sample Variance	438.693
Kurtosis	15.689	Kurtosis	-0.846	Kurtosis	-0.442
Skewness	3.471	Skewness	-0.208	Skewness	-0.032
Range	202.312	Range	73.257	Range	82.014
Minimum	259.685	Minimum	248.947	Minimum	241.774
Maximum	461.997	Maximum	322.204	Maximum	323.789
Sum	8969.184	Sum	8512.290	Sum	8348.115
Count	30	Count	30	Count	30
Confidence Level(95.0%)	13.266	Confidence Level(95.0%)	7.331	Confidence Level(95.0%)	7.821
Porosity					
<i>Top</i>		<i>Middle</i>		<i>Bottom</i>	
Mean	0.093	Mean	0.069	Mean	0.138
Standard Error	0.022	Standard Error	0.037	Standard Error	0.111
Median	0.050	Median	0.029	Median	0.025
Mode	#N/A	Mode	#N/A	Mode	#N/A
Standard Deviation	0.097	Standard Deviation	0.167	Standard Deviation	0.496
Sample Variance	0.009	Sample Variance	0.028	Sample Variance	0.246
Kurtosis	2.447	Kurtosis	19.621	Kurtosis	19.936
Skewness	1.742	Skewness	4.412	Skewness	4.462
Range	0.371	Range	0.764	Range	2.240
Minimum	0.000	Minimum	0.009	Minimum	0.005
Maximum	0.372	Maximum	0.774	Maximum	2.245
Sum	1.855	Sum	1.371	Sum	2.755
Count	20	Count	20	Count	20
Confidence Level(95.0%)	0.046	Confidence Level(95.0%)	0.078	Confidence Level(95.0%)	0.232

APPENDIX L
OXYGEN CONTENT BOX PLOTS

